A

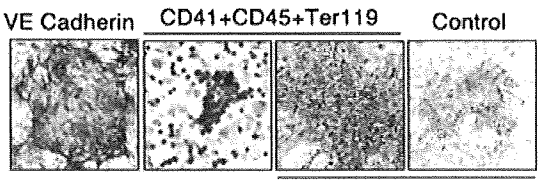

B

Clones	Only one cell 24 hours after sorting	After 5 days		
		HC	EC	HC+EC
DsRed iPS cells (256H18)	361 wells	10 wells (2.7%)	19 wells (5.2%)	8 wells (2.2%)
D3 ES cells	369 wells	9 wells (2.4%)	13 wells (3.5%)	11 wells (2.9%)

HC: Hematopoietic cells
EC: Endothelial cells

Fig. 7. Common hemoangiogenic progenitors are present in Flk-1$^+$ cells during iPS-cell differentiation. A: Single Flk-1$^+$ cells were cultured on OP9 layers in the wells of 96-well plates and immunostained with anti-VE-cadherin antibodies, or a cocktail of anti-CD41, anti-CD45, and anti-Ter119 antibodies, 7 days after sorting. B: Number of wells that showed EC (endothelial cells), HC (hematopoietic cells), and EC + HC development were counted as described in text.

unlimited capacity for self-renewal (Takahashi and Yamanaka, 2006; Meissner et al., 2007; Okita et al., 2007; Park et al., 2007; Takahashi et al., 2007; Yu et al., 2007; Aoi et al., 2008; Hanna et al., 2008; Nakagawa et al., 2008). The use of customized pluripotent stem cells would avoid the controversies surrounding ES cells. A recent study demonstrated that, after additional genetic manipulation and hematopoietic stem/progenitor cell expansion, autologous iPS cells could be used to treat mice with sickle-cell anemia, clearly revealing the advantage of these cells in regenerative medicine (Hanna et al., 2007).

One significant advantage of iPS cells is that cells from each patient can be used to screen drugs or to examine the effects of novel procedures against various diseases. Many diseases have a complex genetic etiology that affects the development, differentiation, and maturation of different tissues and organs, and require an experimental model system to faithfully reproduce their altered developmental processes (Lensch and Daley, 2006). In light of the heterogeneity of disease phenotypes and drug toxicity, it is desirable to establish defined sources of cells for drug discovery and research. In this area, immortalized cell lines and tissue-specific stem/progenitor cells that have been used for such studies are now being replaced by pluripotent stem cells.

The present study demonstrates that murine iPS cells can recapitulate early hematopoietic development in vitro. We confirmed the step-wise development of primitive and definitive hematopoietic cells, as well as endothelial cells, from Flk-1$^+$ hemoangiogenic progenitors, together with the upregulation of genes related to both lineages. Both lineages could be generated from individual Flk-1$^+$ cells, strongly suggesting the existence of common progenitor "hemangioblasts," as was previously reported for ES cells and embryos (Flamme et al., 1995; Risau, 1995; Risau and Flamme, 1995; Choi et al., 1998; Huber et al., 2004).

Step-wise development of primitive and definitive hematopoiesis from iPS-derived intermediate mesodermal progenitors

During embryogenesis, primitive hematopoiesis emerges in the yolk sac on 7.5 d.p.c. Following this process, definitive hematopoiesis, which is the major hematopoietic process throughout life, originates on 8.5 d.p.c. in the AGM region (Muller et al., 1994; Medvinsky and Dzierzak, 1996; Matsuoka et al., 2001). When the site of hematopoiesis shifts to the fetal liver on 10.5 d.p.c. and finally to the bone marrow, the number of blood cells massively increases; erythroid cell lineages are the major products in the fetal liver, and myeloid lineages appear at later stages. Here we demonstrated that Flk-1$^+$ mesodermal cells derived from iPS cells can lead to both primitive and definitive hematopoiesis.

Interestingly, the time courses of the hematopoietic differentiation of iPS and ES cell lines in our experiments were almost precisely synchronized with those seen in embryonic development. Hematopoietic colonies on the OP9 layer were first observed on day 7 of differentiation, and the number of cells produced increased explosively from day 11. Immunostaining and RT-PCR indicated a shift from primitive to definitive hematopoiesis as differentiation progressed over time. Moreover, the results of the MTC colony-forming assay also suggested that hematopoietic differentiation in our system reflects that occurring in embryogenesis: CFU-Mix and BFU-E colonies were mainly observed until day 9, while CFU-GM and CFU-G colonies became dominant on day 11 and thereafter.

Identifying and inducing hematopoietic stem cells (HSCs) in vitro is of great biological interest. Previous studies have suggested that the cobblestone area forming cells (CAFCs) observed in the OP9 system are indicative of the existence of primitive hematopoietic progenitors (Suwabe et al., 1998); CD34, c-kit, and Sca1 are among the characteristic markers of HSCs or very immature progenitors. In our study, we observed CAFCs derived from iPS cells, and FACS analyses revealed that many of the iPS-derived hematopoietic cells expressed the progenitor markers mentioned above. Taken together, these findings suggest that iPS cells can produce very immature hematopoietic progenitors in vitro. In the future, further study will be necessary to investigate whether iPS cells can generate true HSCs that demonstrate long-term multilineage marrow reconstitution in lethally irradiated mice without any additional gene manipulation.

Concomitant differentiation of iPS cells into hematopoietic and endothelial lineages

Several in vivo and in vitro studies have demonstrated a close association between hematopoietic and endothelial differentiation. Previous experiments have shown that murine and primate ES cells differentiate into hematopoietic cells via common Flk1$^+$ hemoangiogenic progenitors (Nishikawa et al., 1998; Umeda et al., 2006). Using RT-PCR and the single-cell deposition assay, our study demonstrated that iPS cells, like ES cells, can generate hematopietic and endothelial cells concomitantly, as is observed in embryogenesis.

The RT-PCR data demonstrated that the expression of the early mesodermal marker *Brachyury* was followed by that of *flk-1* and *scl*, both of which are crucial for the development of common progenitors (Nishikawa et al., 1998; Chung et al., 2002). The expression of genes associated with both lineages began thereafter. These results suggest that the orchestrated process from mesoderm development to the specification of either lineage during embryogenesis is also recapitulated in the iPS-cell model.

The single-deposition assay demonstrated that iPS cells possess an equivalent capacity to ES cells to develop bipotent progenitors at the single cell level. However, the frequency of progenitor development was unexpectedly low. One possible reason for this is the low clonal growth rate in our single-cell culture condition. Another possibility is that the sorted Flk-1$^+$ cells included, besides hemangioblasts, progenitors that contribute to other mesodermal lineages. Recent studies on murine ES and iPS cells demonstrated the development of cardiac muscles, vascular smooth muscles, and pericytes from Flk-1$^+$ fractions (Yamashita et al., 2000; Iida et al., 2005; Baba et al., 2007b; Narazaki et al., 2008). We also observed the formation of contractile colonies from Flk-1$^+$ fractions (data not shown). This may be one alternative reason for the observed low frequency of differentiation of either lineage. Further studies will enhance our understanding of the developmental biology of iPS cells.

Hematopoietic potential of iPS-derived Flk-1$^+$ progenitors is equivalent, regardless of the clone

In our experiments, the efficacy of Flk-1$^+$ cell induction varied between the clones, although the timing of their differentiation was the same. This may be potentially due to contamination by the SNL feeder cells. As these feeder cells were not eliminated at the start of differentiation, they would have remained throughout the assay and might have inhibited differentiation. However, to address these problems, it will be necessary to study the biological characteristics of iPS cells further, including their epigenetic behavior during differentiation. The most interesting and encouraging finding in our study was that the sorted Flk-1$^+$ cells derived from all analyzed iPS and ES clones were similar in their ability to generate hematopoietic cells.

In conclusion, our results demonstrate that iPS cells can develop into hematopoietic cells in vitro via hemoangiogenic progenitors, the so-called "hemangioblasts." Furthermore, iPS cells traverse the primitive and definitive hematopoietic stages in a manner similar to that observed during embryogenesis. Although future investigations at the biological and molecular levels are highly desirable, our study suggests that iPS cells hold great promise in medicine, and may aid in attaining the long sought goal of patient-specific stem cells.

Acknowledgments

This work was supported by grants from the Ministry of Education, Culture, Sports, Science, and Technology of Japan.

Literature Cited

Aoi T, Yae K, Nakagawa M, Ichisaka T, Okita K, Takahashi K, Chiba T, Yamanaka S. 2008. Generation of pluripotent stem cells from adult mouse liver and stomach cells. Science (New York, NY) 321:699–702.

Baba S, Heike T, Umeda K, Iwasa T, Kaichi S, Hiraumi Y, Doi H, Yoshimoto M, Kanatsu-Shinohara M, Shinohara T, Nakahata T. 2007a. Generation of cardiac and endothelial cells from neonatal mouse testis-derived multipotent germline stem cells. Stem Cells (Dayton, Ohio) 25:1375–1383.

Baba S, Heike T, Yoshimoto M, Umeda K, Doi H, Iwasa T, Lin X, Matsuoka S, Komeda M, Nakahata T. 2007b. Flk1(+) cardiac stem/progenitor cells derived from embryonic stem cells improve cardiac function in a dilated cardiomyopathy mouse model. Cardiovasc Res 76:119–131.

Choi K, Kennedy M, Kazarov A, Papadimitriou JC, Keller G. 1998. A common precursor for hematopoietic and endothelial cells. Development (Cambridge, England) 125:725–732.

Chung YS, Zhang WJ, Arentson E, Kingsley PD, Palis J, Choi K. 2002. Lineage analysis of the hemangioblast as defined by FLK1 and SCL expression. Development (Cambridge, England) 129:5511–5520.

Doetschman TC, Eistetter H, Katz M, Schmidt W, Kemler R. 1985. The in vitro development of blastocyst-derived embryonic stem cell lines: Formation of visceral yolk sac, blood islands and myocardium. J Embryol Exp Morphol 87:27–45.

Evans MJ, Kaufman MH. 1981. Establishment in culture of pluripotential cells from mouse embryos. Nature 292:154–156.

Flamme I, Breier G, Risau W. 1995. Vascular endothelial growth factor (VEGF) and VEGF receptor 2 (flk-1) are expressed during vasculogenesis and vascular differentiation in the quail embryo. Dev Biol 169:699–712.

Garcia-Porrero JA, Manaia A, Jimeno J, Lasky LL, Dieterlen-Lievre F, Godin IE. 1998. Antigenic profiles of endothelial and hemopoietic lineages in murine intraembryonic hemogenic sites. Dev Comp Immunol 22:303–319.

Hanna J, Wernig M, Markoulaki S, Sun CW, Meissner A, Cassady JP, Beard C, Brambrink T, Wu LC, Townes TM, Jaenisch R. 2007. Treatment of sickle cell anemia mouse model with iPS cells generated from autologous skin. Science (New York, NY) 318:1920–1923.

Hanna J, Markoulaki S, Schorderet P, Carey BW, Beard C, Wernig M, Creyghton MP, Steine EJ, Cassady JP, Foreman R, Lengner CJ, Dausman JA, Jaenisch R. 2008. Direct reprogramming of terminally differentiated mature B lymphocytes to pluripotency. Cell 133:250–264.

Hansen JN, Konkel DA, Leder P. 1982. The sequence of a mouse embryonic beta-globin gene. Evolution of the gene and its signal region. J Biol Chem 257:1048–1052.

Huber TL, Kouskoff V, Fehling HJ, Palis J, Keller G. 2004. Haemangioblast commitment is initiated in the primitive streak of the mouse embryo. Nature 432:625–630.

Iida M, Heike T, Yoshimoto M, Baba S, Doi H, Nakahata T. 2005. Identification of cardiac stem cells with FLK1, CD31, and VE-cadherin expression during embryonic stem cell differentiation. FASEB J 19:371–378.

Jackson CW. 1973. Cholinesterase as a possible marker for early cells of the megakaryocytic series. Blood 42:413–421.

Jaenisch R, Young R. 2008. Stem cells, the molecular circuitry of pluripotency and nuclear reprogramming. Cell 132:567–582.

Konkel DA, Tilghman SM, Leder P. 1978. The sequence of the chromosomal mouse beta-globin major gene: Homologies in capping, splicing and poly(A) sites. Cell 15:1125–1132.

Ku HT, Zhang N, Kubo A, O'Connor R, Mao M, Keller G, Bromberg JS. 2004. Committing embryonic stem cells to early endocrine pancreas in vitro. Stem Cells (Dayton, Ohio) 22:1205–1217.

Kyba M, Perlingeiro RC, Daley GQ. 2002. HoxB4 confers definitive lymphoid-myeloid engraftment potential on embryonic stem cell and yolk sac hematopoietic progenitors. Cell 109:29–37.

Kyba M, Perlingeiro RC, Hoover RR, Lu CW, Pierce J, Daley GQ. 2003. Enhanced hematopoietic differentiation of embryonic stem cells conditionally expressing Stat5. Proc Natl Acad Sci USA 100:11904–11910.

Leder A, Weir L, Leder P. 1985. Characterization, expression, and evolution of the mouse embryonic zeta-globin gene. Mol Cell Biol 5:1025–1033.

Leder A, Kuo A, Shen MM, Leder P. 1992. In situ hybridization reveals co-expression of embryonic and adult alpha globin genes in the earliest murine erythrocyte progenitors. Development (Cambridge, England) 116:1041–1049.

Lensch MW, Daley GQ. 2006. Scientific and clinical opportunities for modeling blood disorders with embryonic stem cells. Blood 107:2605–2612.

Ling V, Neben S. 1997. In vitro differentiation of embryonic stem cells: Immunophenotypic analysis of cultured embryoid bodies. J Cell Physiol 171:104–115.

Maherali N, Sridharan R, Xie W, Utikal J, Eminli S, Arnold K, Stadtfeld M, Yachechko R, Tchieu J, Jaenisch R, Plath K, Hochedlinger K. 2007. Directly reprogrammed fibroblasts show global epigenetic remodeling and widespread tissue contribution. Cell Stem Cell 1:55–70.

Matsuoka S, Tsuji K, Hisakawa H, Xu M, Ebihara Y, Ishii T, Sugiyama D, Manabe A, Tanaka R, Ikeda Y, Asano S, Nakahata T. 2001. Generation of definitive hematopoietic stem cells from murine early yolk sac and paraaortic splanchnopleures by aorta-gonad-mesonephros region-derived stromal cells. Blood 98:6–12.

Medvinsky A, Dzierzak E. 1996. Definitive hematopoiesis is autonomously initiated by the AGM region. Cell 86:897–906.

Meissner A, Wernig M, Jaenisch R. 2007. Direct reprogramming of genetically unmodified fibroblasts into pluripotent stem cells. Nat Biotechnol 25:1177–1181.

Miwa Y, Atsumi T, Imai N, Ikawa Y. 1991. Primitive erythropoiesis of mouse teratocarcinoma stem cells PCC3/A/1 in serum-free medium. Development (Cambridge, England) 111:543–549.

Moore MA, Metcalf D. 1970. Ontogeny of the haemopoietic system: Yolk sac origin of in vivo and in vitro colony forming cells in the developing mouse embryo. Br J Haematol 18:279–296.

Motro B, van der Kooy D, Rossant J, Reith A, Bernstein A. 1991. Contiguous patterns of c-kit and steel expression: Analysis of mutations at the W and Sl loci. Development (Cambridge, England) 113:1207–1221.

Muller AM, Medvinsky A, Strouboulis J, Grosveld F, Dzierzak E. 1994. Development of hematopoietic stem cell activity in the mouse embryo. Immunity 1:291–301.

Nakagawa M, Koyanagi M, Tanabe K, Takahashi K, Ichisaka T, Aoi T, Okita K, Mochiduki Y, Takizawa N, Yamanaka S. 2008. Generation of induced pluripotent stem cells without Myc from mouse and human fibroblasts. Nat Biotechnol 26:101–106.

Nakahata T, Ogawa M. 1982a. Clonal origin of murine hemopoietic colonies with apparent restriction to granuclocyte-macrophage-megakaryocyte (GMM) differentiation. J Cell Physiol 111:239–246.

Nakahata T, Ogawa M. 1982b. Hemopoietic colony-forming cells in umbilical cord blood with extensive capability to generate mono- and multipotential hemopoietic progenitors. J Clin Invest 70:1324–1328.

Nakahata T, Ogawa M. 1982c. Identification in culture of a class of hemopoietic colony-forming units with extensive capability to self-renew and generate multipotential hemopoietic colonies. Proc Natl Acad Sci USA 79:3843–3847.

Nakanishi M, Kurisaki A, Hayashi Y, Warashina M, Ishiura S, Kusuda-Furue M, Asashima M. 2009. Directed induction of anterior and posterior primitive streak by Wnt from embryonic stem cells cultured in a chemically defined serum-free medium. FASEB J 23:114–122.

Nakano T, Kodama H, Honjo T. 1994. Generation of lymphohematopoietic cells from embryonic stem cells in culture. Science (New York, NY) 265:1098–1101.

Nakano T, Kodama H, Honjo T. 1996. In vitro development of primitive and definitive erythrocytes from different precursors. Science (New York, NY) 272:722–724.

Narazaki G, Uosaki H, Teranishi M, Okita K, Kim B, Matsuoka S, Yamanaka S, Yamashita JK. 2008. Directed and systematic differentiation of cardiovascular cells from mouse induced pluripotent stem cells. Circulation 118:498–506.

Nishikawa SI, Nishikawa S, Hirashima M, Matsuyoshi N, Kodama H. 1998. Progressive lineage analysis by cell sorting and culture identifies FLK1+VE-cadherin+ cells at a diverging point of endothelial and hemopoietic lineages. Development (Cambridge, England) 125:1747–1757.

Nishioka Y, Leder P. 1979. The complete sequence of a chromosomal mouse alpha-globin gene reveals elements conserved throughout vertebrate evolution. Cell 18:875–882.

Okita K, Ichisaka T, Yamanaka S. 2007. Generation of germline-competent induced pluripotent stem cells. Nature 448:313–317.

Park IH, Zhao R, West JA, Yabuuchi A, Huo H, Ince TA, Lerou PH, Lensch MW, Daley GQ. 2007. Reprogramming of human somatic cells to pluripotency with defined factors. Nature 451:141–146.

Redmond LC, Dumur CI, Archer KJ, Haar JL, Lloyd JA. 2008. Identification of erythroid-enriched gene expression in the mouse embryonic yolk sac using microdissected cells. Dev Dyn 237:436–446.

Risau W. 1995. Differentiation of endothelium. FASEB J 9:926–933.
Risau W, Flamme I. 1995. Vasculogenesis. Annu Rev Cell Dev Biol 11:73–91.
Shalaby F, Ho J, Stanford WL, Fischer KD, Schuh AC, Schwartz L, Bernstein A, Rossant J. 1997. A requirement for Flk1 in primitive and definitive hematopoiesis and vasculogenesis. Cell 89:981–990.
Shimizu R, Takahashi S, Ohneda K, Engel JD, Yamamoto M. 2001. In vivo requirements for GATA-1 functional domains during primitive and definitive erythropoiesis. EMBO J 20:5250–5260.
Shimizu R, Kuroha T, Ohneda O, Pan X, Ohneda K, Takahashi S, Philipsen S, Yamamoto M. 2004. Leukemogenesis caused by incapacitated GATA-1 function. Mol Cell Biol 24:10814–10825.
Shinoda G, Umeda K, Heike T, Arai M, Niwa A, Ma F, Suemori H, Luo HY, Chui DH, Torii R, Shibuya M, Nakatsuji N, Nakahata T. 2007. alpha4-Integrin(+) endothelium derived from primate embryonic stem cells generates primitive and definitive hematopoietic cells. Blood 109:2406–2415.
Suwabe N, Takahashi S, Nakano T, Yamamoto M. 1998. GATA-1 regulates growth and differentiation of definitive erythroid lineage cells during in vitro ES cell differentiation. Blood 92:4108–4118.
Takahashi K, Yamanaka S. 2006. Induction of pluripotent stem cells from mouse embryonic and adult fibroblast cultures by defined factors. Cell 126:663–676.
Takahashi K, Tanabe K, Ohnuki M, Narita M, Ichisaka T, Tomoda K, Yamanaka S. 2007. Induction of pluripotent stem cells from adult human fibroblasts by defined factors. Cell 131:861–872.
Umeda K, Heike T, Yoshimoto M, Shiota M, Suemori H, Luo HY, Chui DH, Torii R, Shibuya M, Nakatsuji N, Nakahata T. 2004. Development of primitive and definitive hematopoiesis from nonhuman primate embryonic stem cells in vitro. Development (Cambridge, England) 131:1869–1879.
Umeda K, Heike T, Yoshimoto M, Shinoda G, Shiota M, Suemori H, Luo HY, Chui DH, Torii R, Shibuya M, Nakatsuji N, Nakahata T. 2006. Identification and characterization of hemoangiogenic progenitors during cynomolgus monkey embryonic stem cell differentiation. Stem Cells (Dayton, Ohio) 24:1348–1358.
van de Rijn M, Heimfeld S, Spangrude GJ, Weissman IL. 1989. Mouse hematopoietic stem-cell antigen Sca-1 is a member of the Ly-6 antigen family. Proc Natl Acad Sci USA 86:4634–4638.
Vodyanik MA, Slukvin II. 2007. Hematoendothelial differentiation of human embryonic stem cells. Curr Protoc Cell Biol Chapter 23:Unit 23.6.
Vodyanik MA, Bork JA, Thomson JA, Slukvin II. 2005. Human embryonic stem cell-derived CD34+ cells: Efficient production in the coculture with OP9 stromal cells and analysis of lymphohematopoietic potential. Blood 105:617–626.
Wood HB, May G, Healy L, Enver T, Morriss-Kay GM. 1997. CD34 expression patterns during early mouse development are related to modes of blood vessel formation and reveal additional sites of hematopoiesis. Blood 90:2300–2311.
Woodard JP, Gulbahce E, Shreve M, Steiner M, Peters C, Hite S, Ramsay NK, DeFor T, Baker KS. 2000. Pulmonary cytolytic thrombi: A newly recognized complication of stem cell transplantation. Bone Marrow Transplant 25:293–300.
Xu MJ, Matsuoka S, Yang FC, Ebihara Y, Manabe A, Tanaka R, Eguchi M, Asano S, Nakahata T, Tsuji K. 2001. Evidence for the presence of murine primitive megakaryocytopoiesis in the early yolk sac. Blood 97:2016–2022.
Yamashita J, Itoh H, Hirashima M, Ogawa M, Nishikawa S, Yurugi T, Naito M, Nakao K. 2000. Flk1-positive cells derived from embryonic stem cells serve as vascular progenitors. Nature 408:92–96.
Yang FC, Tsuji K, Oda A, Ebihara Y, Xu MJ, Kaneko A, Hanada S, Mitsui T, Kikuchi A, Manabe A, Watanabe S, Ikeda Y, Nakahata T. 1999. Differential effects of human granulocyte colony-stimulating factor (hG-CSF) and thrombopoietin on megakaryopoiesis and platelet function in hG-CSF receptor-transgenic mice. Blood 94:950–958.
Yu J, Vodyanik MA, Smuga-Otto K, Antosiewicz-Bourget J, Frane JL, Tian S, Nie J, Jonsdottir GA, Ruotti V, Stewart R, Slukvin II, Thomson JA. 2007. Induced pluripotent stem cell lines derived from human somatic cells. Science (New York, NY) 318:1917–1920.

Published May 11, 2009

Mast cells mediate neutrophil recruitment and vascular leakage through the NLRP3 inflammasome in histamine-independent urticaria

Yuumi Nakamura,[1] Naotomo Kambe,[1] Megumu Saito,[2] Ryuta Nishikomori,[2] Yun-Gi Kim,[3] Makoto Murakami,[4] Gabriel Núñez,[3] and Hiroyuki Matsue[1]

[1]Department of Dermatology, Chiba University Graduate School of Medicine, Chuo-ku, Chiba 260-8670, Japan
[2]Department of Pediatrics, Kyoto University Graduate School of Medicine, Sakyo-ku, Kyoto 606-8507, Japan
[3]Department of Pathology and Comprehensive Cancer Center, University of Michigan Medical School, Ann Arbor, MI 48109
[4]Biomembrane Signaling Project, The Tokyo Metropolitan Institute of Medical Science, Bunkyo-ku, Tokyo 113-8613, Japan

Urticarial rash observed in cryopyrin-associated periodic syndrome (CAPS) caused by nucleotide-binding oligomerization domain–leucine-rich repeats containing pyrin domain 3 (NLRP3) mutations is effectively suppressed by anti–interleukin (IL)-1 treatment, suggesting a pathophysiological role of IL-1β in the skin. However, the cellular mechanisms regulating IL-1β production in the skin of CAPS patients remain unclear. We identified mast cells (MCs) as the main cell population responsible for IL-1β production in the skin of CAPS patients. Unlike normal MCs that required stimulation with proinflammatory stimuli for IL-1β production, resident MCs from CAPS patients constitutively produced IL-1β. Primary MCs expressed inflammasome components and secreted IL-1β via NLRP3 and apoptosis-associated speck-like protein containing a caspase recruitment domain when stimulated with microbial stimuli known to activate caspase-1. Furthermore, MCs expressing disease-associated but not wild-type NLRP3 secreted IL-1β and induced neutrophil migration and vascular leakage, the histological hallmarks of urticarial rash, when transplanted into mouse skin. Our findings implicate MCs as IL-1β producers in the skin and mediators of histamine-independent urticaria through the NLRP3 inflammasome.

CORRESPONDENCE
Naotomo Kambe:
nkambe@faculty.chiba-u.jp

Abbreviations used: Ab, antibody; ASC, apoptosis-associated speck-like protein containing a caspase recruitment domain; BMCMC, bone marrow–derived cultured MC; CAPS, cryopyrin-associated periodic syndrome; FSMC, fetus skin–derived MC; LRR, leucine-rich repeat; MC, mast cell; MIM, Mendelian inheritance in men number; MWS, Muckle-Wells syndrome; NLRP3, NOD-LRRs containing pyrin domain 3; NOD, nucleotide-binding oligomerization domain; P2X7R, purinergic P2X, ligand-gated ion channel 7 receptor; PAMP, pathogen-associated molecular pattern.

Urticaria, or hives, is a common disease that can affect up to 20% of the general population (1). Chronic urticaria, defined as urticaria that persists for >6 wk, occurs in 0.1% of the population (2), and in a significant percentage of cases (~40–80%), there is no identifiable cause (1, 3). H1 antihistamines have remained the first line of treatment because histamine release from cutaneous mast cells (MCs) plays an important role in the pathophysiology of urticaria development. However, only ~55% of patients with chronic urticaria are responsive to antihistamines (4), suggesting that in a significant number of individuals, chronic urticaria is mediated via histamine-independent mechanisms.

An urticarial rash developing in the neonatal or early infantile period is one of the clinical manifestations characteristic of cryopyrin-associated periodic syndrome (CAPS). CAPS consists of a spectrum of hereditary periodic fever disorders that comprise three phenotypically overlapping but relatively distinct syndromes: familial cold autoinflammatory syndrome (Mendelian inheritance in men number [MIM] 120100), Muckle-Wells syndrome (MWS; MIM 191900), and chronic infantile neurological cutaneous and articular syndrome (MIM 607115), which is also known as neonatal-onset multisystem inflammatory disease. Familial cold autoinflammatory syndrome and MWS are characterized by periodic attacks of urticarial rash, fever, and arthralgia, whereas patients with chronic infantile neurological cutaneous and articular syndrome, the most severe form of CAPS, exhibit chronic urticaria as well as fever, arthropathy, chronic meningitis, papilledema, growth and mental retardation, and

The Rockefeller University Press $30.00
J. Exp. Med. Vol. 206 No. 5 1037-1046
www.jem.org/cgi/doi/10.1084/jem.20082179

Supplemental Material can be found at:
http://jem.rupress.org/content/suppl/2009/04/13/jem.20082179.DC1.html
http://jem.rupress.org/content/suppl/2009/05/04/jem.20082179.DC2.html

Published May 11, 2009

hearing loss (5). The urticarial rash observed in CAPS is similar to that associated with common urticaria. However, unlike the latter disorder, the rash observed in most CAPS patients responds to therapy with IL-1 receptor antagonist rather than antihistamines, suggesting that urticaria in these patients is mediated by IL-1. However, the cellular mechanism responsible for urticaria in CAPS patients remains poorly understood.

The mature form of IL-1β is produced by cleavage of the inactive pro–IL-1β precursor by caspase-1, a protease activated by a large multiprotein complex termed the inflammasome (6). CAPS is caused by missense mutations in the gene, nucleotide-binding oligomerization domain (NOD)–leucine-rich repeats (LRRs) containing pyrin domain 3 (*NLRP3*) (7), whose product is a component of the inflammasome that includes the adaptor protein, apoptosis-associated speck-like protein containing a caspase recruitment domain (ASC), and procaspase-1 (8, 9). NLRP3, a member of the NOD-like receptor family, is an intracellular receptor involved in the recognition of pathogen-associated molecular patterns (PAMPs). Although several microbial activators of NLRP3 have been reported, the precise mechanism by which the NLRP3 inflammasome is activated by PAMPs remains poorly understood. In the presence of ATP or pore-forming molecules, several PAMPs, including LPS, muramyl dipeptide, bacterial mRNA, and the antiviral compound R837, activate the NLRP3 inflammasome (10, 11). In addition to PAMPs, NLRP3 senses endogenous danger signals such as monosodium urate crystals and particulate matter including asbestos, silica (12), and aluminum salts (13, 14). Disease-associated NLRP3 mutations associated with CAPS localize to the centrally located NOD domain and constitutively activate caspase-1 to produce active IL-1β (8, 15). NLRP3 is predominantly expressed in monocytes, granulocytes, and chondrocytes (16, 17), but to date, no reports have investigated the cells in the skin that are involved in the development of urticarial rash associated with CAPS. Our study identifies resident MCs in the skin as a cell population capable of producing IL-1β via the NLRP3 inflammasome and provides evidence that MCs mediate urticarial rash via dysregulated IL-1β production in the skin of CAPS patients.

RESULTS

Resident MCs produce constitutively mature IL-1β in CAPS skin

To identify the source of IL-1β in the human skin, we performed immunolabeling of skin organ cultures with an antibody (Ab) that recognizes p17, the mature form of IL-1β. Expression of mature IL-1β was undetectable in normal skin cells but was induced in resident cells by incubation of skin organ cultures with LPS and R837 (Fig. 1). In contrast, cells in the dermis of two MWS patients harboring the E567K or K355T *NLRP3* mutation and suffering from active disease but not receiving any treatment expressed the mature form of IL-1β constitutively without any stimulation (Fig. 1). Notably, the majority of the mature IL-1β–positive cells colocalized with avidin-FITC (Fig. 1), which specifically labels tryptase-positive MCs, but not with HLA-DR, -DP, -DQ, a marker of DCs and macrophages (Fig. S1), in both normal and CAPS skin.

MCs express inflammasome components and produce IL-1β in response to proinflammatory stimuli

We next analyzed the expression of inflammasome components in MCs using mouse bone marrow–derived cultured MCs (BMCMCs). The purity of cultured MCs, which was >97%, was confirmed by surface expression of CD45 and Kit, as well as FITC-avidin labeling. Exclusion of DCs/macrophages was further supported by the lack of I-A^b expression in the MC population (Fig. S2 A). BMCMCs constitutively expressed *Casp1* and the critical adaptor *Asc*, as determined

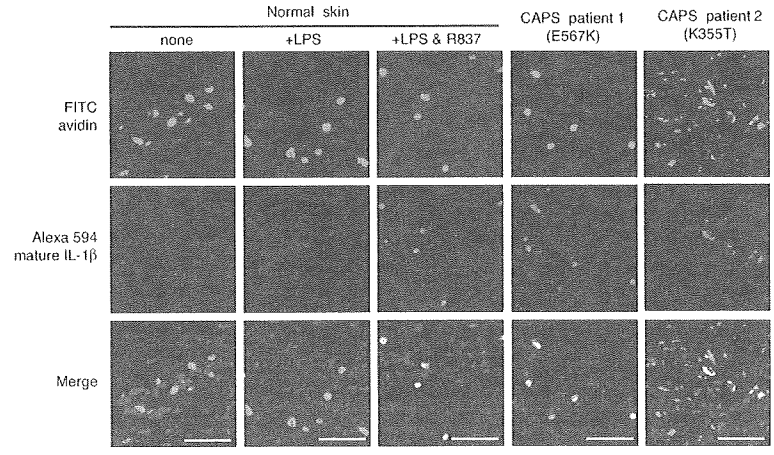

Figure 1. MCs from the skin of CAPS patients expressing disease-associated NLRP3 mutations constitutively express the mature form of IL-1β. Human skin specimens were stained with FITC-avidin to label MCs (top) and Alexa Fluor 594–conjugated anti–IL-1β Ab that recognizes only the mature form of IL-1β (middle). (bottom) Overlay of fluorescence images of the top and middle panels. The nuclei were counterstained with Hoechst 33342 (blue). Normal skin represents organ skin cultures with or without incubation with 100 ng/ml LPS or LPS and 100 µM R837 for 24 h. Results are representative of at least three separate experiments. Bars, 50 µm.

Published May 11, 2009

by RT-PCR analysis (Fig. 2, A and B). In contrast, there was no or little expression of *Nlrp3* and *Il1b* in MCs, but both genes were induced by stimulation with LPS (Fig. 2, A and B), which is consistent with what was reported in human monocytes (18). Induction of *Nlrp3* and *Il1b* by LPS was reduced by treatment with MG-132, a broad proteasome inhibitor that can affect several signaling pathways including NF-κB (Fig. 2 A), suggesting that induction of *Nlrp3* and *Il1b* may require NF-κB activation.

We next determined the ability of MCs to produce IL-1β in response to proinflammatory stimuli known to activate caspase-1. Stimulation of MCs with LPS alone induced little IL-1β secretion, whereas treatment with R837, a small antiviral synthetic compound that activates the NLRP3 inflammasome (11), induced potent IL-1β secretion in MCs pretreated with LPS (Fig. 2, C and D). In accordance with these results, R837 effectively induced intracellular processing of pro–IL-1β into p17 in LPS-primed MCs, whereas secretion of mature IL-1β into the culture supernatant was more potently induced by ATP than by R837 (Fig. 2 D). BMCMCs did not express *Tlr7* mRNA as assessed by real-time PCR (not depicted) and Tlr7 protein by immunoblotting (Fig. S2 B), suggesting that R837 promotes caspase-1 activation independently of Tlr7 in MCs. In contrast, incubation of MCs with LPS alone was sufficient to induce secretion of TNF-α and IL-6 (Fig. 2, E and F). Notably, co-stimulation with LPS and R837 did not induce MC degranulation as determined by the release of β-hexosaminidase (Fig. 2 G) and histamine (Fig. 3 A, right), indicating that the mechanisms involved in IL-1β secretion and degranulation are differentially regulated in MCs.

ATP stimulation through the purinergic P2X, ligand-gated ion channel 7 receptor (P2X7R) is essential for the activation of the NLRP3 inflammasome in macrophages (10, 19). We found that in addition to R837, ATP induced secretion of IL-1β in MCs stimulated with LPS (Fig. 2 D; and Fig. 3 A, left), which is consistent with the expression of the P2x7r in MCs (20). K^+ efflux induced by ATP is important for caspase-1 activation via P2x7r (21), and this ion channel rapidly transitions to a pore-like structure that allows passage of molecules as large as 900 D (19). Notably, IL-1β secretion induced by ATP or R837 was completely abrogated when the MCs were incubated in medium containing a high K^+ concentration (Fig. 3 B). Furthermore,

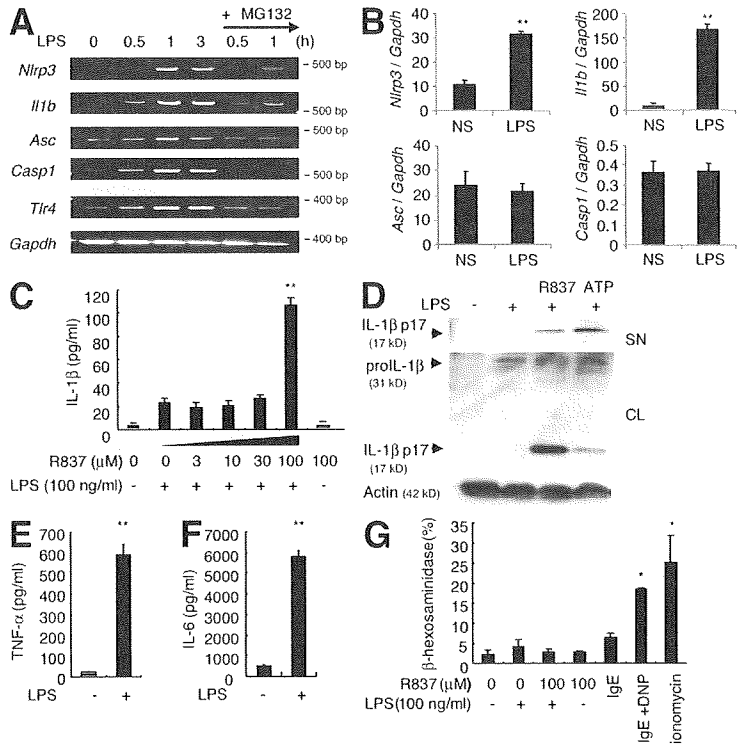

Figure 2. Activation of inflammasome with LPS and R837 induces IL-1β secretion but not degranulation in MCs. (A) Semiquantitative RT-PCR analysis of *Nlrp3*, *Il1b*, *Asc*, *Casp1*, and *Tlr4* in mouse BMCMCs stimulated with 100 ng/ml LPS. 5 μM MG132 was added 30 min before LPS stimulation. (B) Expression of specific mRNAs after stimulation for 3 h with 100 ng/ml LPS in BMCMCs was quantified by real-time PCR and normalized to *Gapdh* expression ($\times 10^4$). (C) BMCMCs were pretreated with LPS for 15 h and stimulated by R837 for 30 min. IL-1β levels in supernatants were measured by ELISA. (D) Immunoblot analysis of cultured supernatant (SN) and cell lysate (CL) from BMCMCs incubated with the indicated stimuli. (E and F) BMCMCs were stimulated with 100 ng/ml LPS for 15 h, and the amounts of TNF-α and IL-6 in culture supernatants were measured by ELISA. (G) Degranulation of BMCMCs was assessed by the release of β-hexosaminidase. Error bars represent means ± SD of triplicates. All results are representative of at least three separate experiments. *, $P < 0.005$; and **, $P < 0.001$ compared with untreated BMCMCs. NS, not stimulated.

Published May 11, 2009

ATP induced large pore formation in MCs as determined by YoPro-1 staining (Fig. 3 C, left), which was not observed in P2x7r-deficient MCs (Fig. 3 C, right). Unlike ATP, R837 did not induce large pore formation (Fig. 3 C, left) even though R837 is structurally related to ATP. However, secretion of IL-1β induced by ATP required expression of P2x7r in LPS-stimulated MCs as well as that elicited by R837 was also dependent, at least in part, on P2x7r (Fig. 3 D). These results suggest that the P2x7r and K^+ efflux are important for both ATP- and R837-induced secretion of IL-1β in MCs.

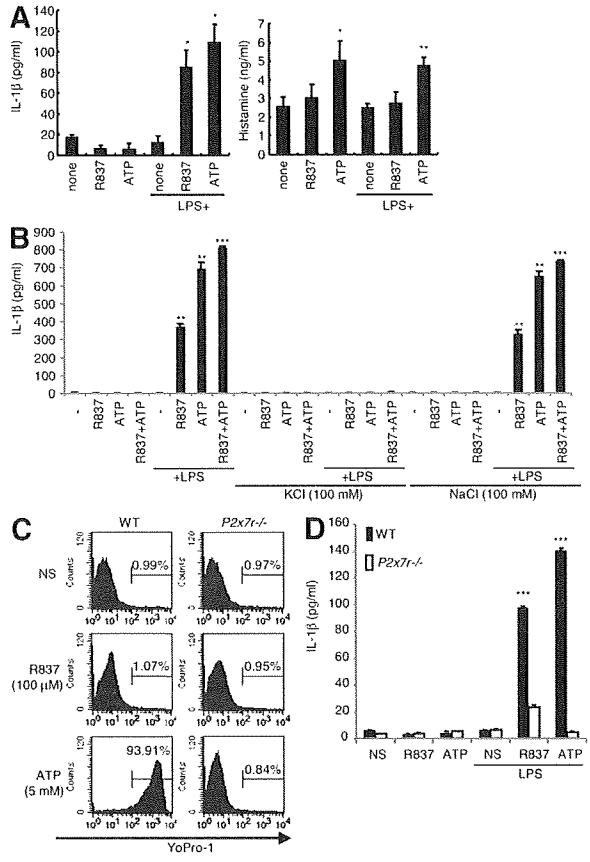

Figure 3. IL-1β secretion induced by R837 and ATP is mediated via P2x7r and K^+ efflux in MCs. (A, left) IL-1β secretion from BMC-MCs. BMCMCs were cultured with or without LPS for 15 h and then stimulated with 5 mM ATP or 100 μM R837. (right) Histamine release from BMCMCs was analyzed by ELISA (same samples as in the left panel). (B) BMCMCs were cultured with or without LPS for 15 h. Medium containing 100 mM KCl or 100 mM NaCl was added for the last 30 min of culture at the same time as ATP or R837. IL-1β was measured in cell-free supernatants. (C) 2 mM YoPro-1 was added 10 min before BMCMCs were left untreated (NS) or stimulated with 5 mM ATP or 100 μM R837 for 30 min, and fluorescence intensity was analyzed by FACS. (D) BMC-MCs were incubated with the indicated stimuli, and IL-1β was measured in cell-free supernatants. Error bars represent means ± SD of triplicates. All results are representative of at least three separate experiments. *, $P < 0.005$; **, $P < 0.001$; and ***, $P < 0.0001$ compared with untreated BMCMCs or between WT and mutant MCs. NS, not stimulated.

IL-1β secretion from MCs depends on the Nlrp3 inflammasome

To determine if the inflammasome is required for IL-1β secretion in MCs, we prepared MCs from WT and mutant mice deficient in Nlrp3, Nlrc4, or Asc. Stimulation of WT and mutant MCs lacking Nlrc4, a NOD-like receptor family member involved in inflammasome activation in response to flagellin (22, 23), induced processing of procaspase-1 into the mature p20 fragment (Fig. 4 A, top). In contrast, production of the processed p20 caspase-1 subunit was impaired in MCs deficient in Nlrp3 or Asc (Fig. 4 A, middle and bottom). Consistently, IL-1β secretion was not detected in MCs from Nlrp3- or Asc-deficient mice in response to LPS plus ATP or R837 (Fig. 4 B, top), whereas that produced by MCs lacking Nlrc4 was unimpaired when compared with WT MCs (Fig. S3, top). The lack of IL-1β secretion in MCs deficient in Nlrp3 or Asc was specific in that production of TNF-α and IL-6 was maintained in WT and mutant MCs (Fig. 4 B, middle and bottom; and Fig. S3, middle and bottom), although the amounts of both cytokines was reduced in MCs lacking Nlrp3 (Fig. 4 B, middle and bottom).

We next assessed the expression of inflammasome components in other populations of MCs. In mice, MCs are often divided into connective tissue– and mucosal-type MCs. Mouse fetus skin–derived MCs (FSMCs) are often used as a model of connective tissue–type MCs (24) that are distributed

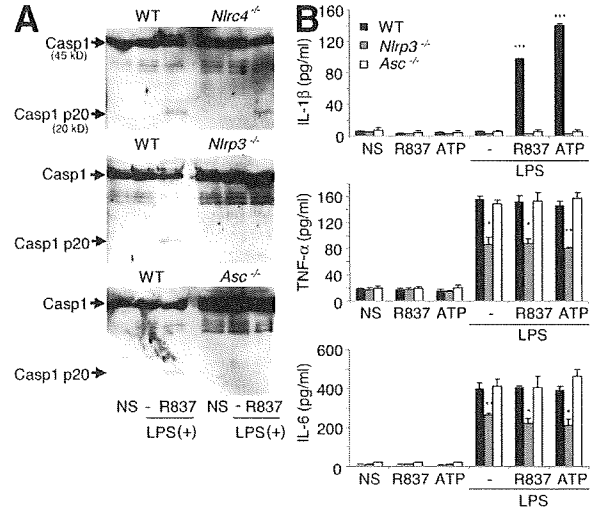

Figure 4. Activation of caspase-1 and IL-1β secretion requires the Nlrp3 inflammasome in MCs. (A) Immunoblot analysis of total cell extracts and supernatant from BMCMCs. Processing of procaspase-1 induced by R837 in LPS-primed BMCMCs from WT, Nlrc4-deficient (*Nlrc4*$^{-/-}$), Nlrp3-deficient (*Nlrp3*$^{-/-}$), and Asc-deficient (*Asc*$^{-/-}$) mice. Cells were pretreated with 100 ng/ml LPS and then stimulated with 100 μM R837. Casp1, procaspase-1; Casp1 p20, cleaved product of caspase-1. (B) Secretion of IL-1β, TNF-α, and IL-6 by LPS-stimulated BMCMCs from the indicated mice in response to R837 or ATP. Error bars represent means ± SD of triplicates. All results are representative of at least three separate experiments. *, $P < 0.005$; **, $P < 0.001$; and ***, $P < 0.0001$ compared between WT and mutant MCs. NS, not stimulated.

Published May 11, 2009

in the dermis. We found that the expression of *Nlrp3*, *Asc*, and *Il1b* was low in unstimulated FSMCs but enhanced after LPS treatment, as it was shown in BMCMCs (Fig. S4 A). Similarly, the pattern of IL-1β secretion and MC degranulation was comparable in BMCMCs and FSMCs (Fig. S4, B and C). Likewise, human MCs derived from cord blood progenitors cultured with stem cell factor expressed *ASC*, *NLRP3*, and *IL1B* after LPS stimulation (Fig. S5 A). Similar to that reported in human monocytes (25), incubation of human MCs with LPS alone was sufficient to induce the processing of pro–IL-1β into the mature form of IL-1β (p17), which was enhanced by R837 or ATP (Fig. S5, B and C).

Constitutive activation of the inflammasome by disease-associated Nlrp3 mutants in MCs

CAPS-associated NLRP3 mutations exhibit constitutive ASC-dependent NF-κB activation when expressed in tumor cell lines (17, 26). To assess the function of mutant NLRP3, we generated mouse Nlrp3 mutants (R258W, D301N, and Y570C) corresponding to the major CAPS-associated mutations (R260W, D303N, and Y570C, respectively) and tested their ability to induce NF-κB activation by luciferase reporter assay. In agreement with human studies, all three Nlrp3 mouse mutants as well as the Nlrp3 mutant lacking the LRR exhibited constitutive Asc-dependent NF-κB activation in HEK293 cells (Fig. 5 A). To further assess the function of disease-associated mutants, we introduced WT and mutant Nlrp3 into BMCMCs using a retroviral expression system that simultaneously coexpresses GFP. After normalization for the number of GFP-expressing cells, we found that the secretion of IL-1β was significantly higher in MCs producing disease-associated Nlrp3 mutants than in cells expressing WT protein after stimulation with LPS (Fig. 5 B). Notably, the increased production of IL-1β induced by Nlrp3 mutants R258W and Y570C was abolished when their pyrin domain was deleted (ΔPYD_R258W and ΔPYD_Y570C; Fig. 5 B), which is consistent with a critical role for the pyrin domain in the interaction with caspase-1 through the adaptor Asc.

To further study the function of disease-associated Nlrp3 mutant in MCs, we stably expressed WT and the common R258W mutant in the MC line MC/9 by retroviral infection (Fig. S6). MC/9 cells constitutively expressed *Nlrp3*, *Asc*, *Casp1*, and *Tlr4* but little or no *Il1b* in the absence of LPS (Fig. 5 C). Expression of *Il1b* was induced by LPS (Fig. 5 C). Importantly, unlike MC/9 cells expressing the CAPS-associated R258W mutant, cells transduced with control GFP vector or producing WT-Nlrp3 required stimulation with both LPS and ATP or R837, two stimuli that activate the Nlrp3

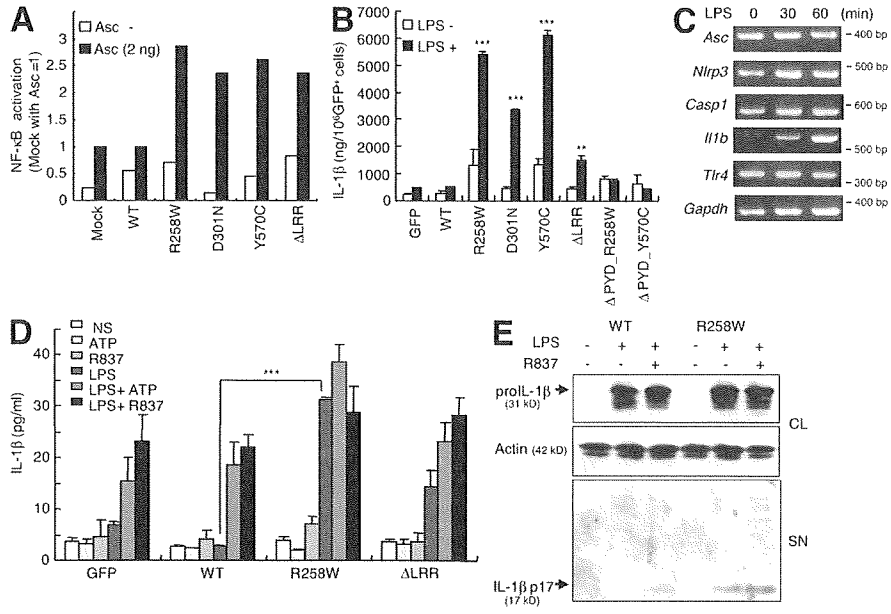

Figure 5. Expression of disease-associated Nlrp3 mutants induce constitutive activation of the inflammasome in MCs. (A) Constructs expressing WT, mutants (R258W, D301N, and Y570C), or Nlrp3 lacking LRR (ΔLRR) were transfected in the presence and absence of Asc plasmid into HEK293 cells. NF-κB activation was assessed by a dual luciferase reporter assay. Values represent the fold increase over that observed by transfection with control or Asc plasmid alone, which was considered as 1. (B) BMCMCs expressing GFP, WT, mutants, and mutants lacking the pyrin (ΔPYD_R258W and ΔPYD_Y570C) by retroviral infection were stimulated with LPS or left untreated. IL-1β was measured by ELISA and normalized to the number of GFP⁺ cells, as previously described (reference 47). **, $P < 0.001$; and ***, $P < 0.0001$ versus LPS-stimulated BMCMCs transfected with WT plasmid. (C) RT-PCR for gene expression in MC/9 cells stimulated with LPS. (D) MC/9 cells stably expressing GFP, WT, mutant Nlrp3, or ΔLRR were stimulated with LPS for 15 h, and then stimulated with ATP or R837. IL-1β secretions were measured by ELISA. ***, $P < 0.0001$ versus LPS-stimulated MC/9 cells expressing WT plasmid. Error bars in B and D represent means ± SD of triplicates. (E) Immunoblot analysis of culture supernatant (SN) and cell lysate (CL) from MC/9 cells stably expressing WT or R258W, and incubated with the indicated stimuli. All results are representative of at least three separate experiments.

Published May 11, 2009

inflammasome, for IL-1β secretion (Fig. 5 D). Although stimulation with LPS alone induced the production of pro–IL-1β in MC/9 cells expressing either WT or mutant Nlrp3, the processed p17 form of mature IL-1β could be detected only in the culture supernatant of MC/9 cells expressing the R258W mutant (Fig. 5 E). In contrast and consistent with results presented in Figs. 2–4, the secretion of mature IL-1β in MC/9 cells expressing WT-Nlrp3 required stimulation with both LPS and R837, which was enhanced in cells producing the CAPS-associated Nlrp3 mutant (Fig. 5 E).

To assess the effect of disease-associated Nlrp3 in vivo, we injected MC/9 cells expressing either WT or mutant Nlrp3 i.p. into mice and assessed the recruitment of neutrophils in the i.p. cavity. FACS analysis revealed that MC/9 cells expressing mutant R258W but not WT-Nlrp3 constitutively produced intracellular IL-1β after injection into the peritoneal cavity (Fig. 6 A). At 36 h after injection, the number of Gr-1$^+$ neutrophils was significantly increased in the peritoneal cavity of mice injected with MC/9 cells expressing mutant R258W-Nlrp3 compared with that found in mice injected with cells expressing WT-Nlrp3 (Fig. 6 B). In contrast, administration of ionomycin, but not MCs expressing WT or mutant Nlrp3, increased the levels of histamine in the peritoneal cavity (Fig. 6 C). Collectively, these results indicate that disease-associated Nlrp3 mutants induce constitutive production of IL-1β but not histamine release, and promote neutrophil recruitment when expressed in MCs.

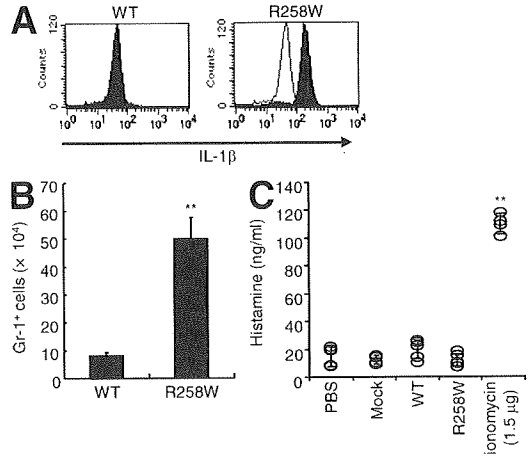

Figure 6. MCs expressing disease-associated Nlrp3 mutant promote neutrophil recruitment but not histamine release in the mouse peritoneal cavity. MC/9 cells stably expressing WT or R258W-Nlrp3 were injected into the mouse peritoneal cavity. Results were obtained 36 h after injection. (A) Shaded histograms represent intracellular IL-1β expression in MC/9 cells. The open histogram corresponds to labeling with isotype-matched control Ab. (B) Gr-1$^+$ cells in the peritoneal fluid. (C) The amounts of histamine in the peritoneal cavity 36 h after the injection of MC/9 cells. As a positive control, 1.5 μg ionomycin was injected 15 min before sample collection. Error bars represent means ± SD of triplicates. All results are representative of at least three separate experiments. **, $P < 0.001$ ($n = 5$ mice per group).

Induction of neutrophil-rich inflammation and vascular leakage by MCs expressing disease-associated Nlrp3 mutant

Urticarial rash in CAPS skin is characterized histologically by the presence of neutrophils and edema in the dermis (27). To study the role of IL-1β produced by MCs in vivo, we injected MC/9 cells expressing WT or mutant Nlrp3 (R258W) into the mouse skin. Histopathological analysis revealed the presence of neutrophils and edema in the dermis of the mouse ear at the site of injection, with MC/9 cells expressing R258W-Nlrp3 in a pattern that was similar to that observed in the involved skin of human CAPS (Fig. 7 A). In contrast, injection with MC/9 cells expressing WT-Nlrp3 induced minimal or no neutrophilic infiltrate or edema in the dermis of the mouse ear (Fig. 7 A). Furthermore, there was enhanced expression of IL-1β in the skin of the ear injected with MC/9 cells expressing R258W when compared with that observed with injection of MC/9 cells producing WT-Nlrp3 (Fig. 7 B). To determine whether the R258W-Nlrp3 mutation promotes vascular leakage, a hallmark of urticaria, we injected mice with MC/9 cells expressing WT and mutant Nlrp3 (R258W) in the ear skin and measured vascular leakage by Evans blue dye. Vascular leakage was significantly higher in the skin of mice injected with MC/9 cells expressing R258W-Nlrp3 than with cells expressing GFP alone or WT-Nlrp3 (Fig. 8, A and B). These results indicate that MCs expressing disease-associated Nlrp3 promote neutrophil recruitment and vascular leakage in the skin, two histological hallmarks of urticarial rash associated with CAPS.

DISCUSSION

MCs are widely distributed throughout vascularized tissues, where they are located near epithelial surfaces that are exposed to environmental cues, including the skin, airways, and gastrointestinal tract (28). MCs are known to promote inflammation and tissue remodeling in IgE-associated allergic disorders as well as to produce multiple cytokines, including IL-1β, in response to microbial stimuli, although the mechanisms involved remained unknown (29, 30). In this paper, we provide evidence that MCs express components of the inflammasome, and these factors are critical for the activation of caspase-1 and IL-1β secretion.

Our analysis revealed that Nlrp3 mutations associated with CAPS induce constitutive activation of the inflammasome in MCs, leading to dysregulated IL-1β production in the skin. These studies are consistent with a previous report that showed enhanced production of IL-1β in the skin of CAPS patients (31), although the cellular source of IL-1β was not investigated by the authors. We showed that transfer of MCs expressing the CAPS-associated Nlrp3 mutant induces perivascular neutrophil-rich inflammation in the mouse skin, which is the histological hallmark of the urticarial rash observed in CAPS patients. Collectively, these studies implicate MCs in inflammasome activation and the pathogenesis of IL-1β–mediated disease in the skin. Because MCs reside in multiples tissues and also participate in experimental models of arthritis (32) and encephalomyelitis (33–35), it is possible that these cells play a role in disease pathogenesis not only in

Published May 11, 2009

the skin but also in the joints and central nervous system, which are also major disease targets in CAPS patients (36). Further studies are needed to better understand the contribution of MCs to IL-1β–mediated disease in autoinflammatory syndromes associated with NLRP3 mutations.

The mechanism by which NLRP3 mutations cause inflammatory diseases is still poorly understood. Studies in vitro suggested that these mutations exert a gain-of-function effect, probably through the loss of a regulatory step associated with NLRP3 activation (6, 8). Consistently, mouse Nlrp3 mutants, corresponding to those observed in human CAPS, induced constitutive Asc-dependent NF-κB activation and IL-1β secretion. Notably, the increased production of IL-1β induced by CAPS-associated Nlrp3 mutants was abolished when their pyrin domain was deleted, which is in accordance with a critical role for that module in the interaction with caspase-1 and assembly of the inflammasome (6, 8).

As is the case with macrophages, production of mature IL-1β via the Nlrp3/Asc inflammasome in mouse MCs required two signals, LPS and ATP or R837. Although a main function of LPS is to induce pro–IL-1β production, LPS also promoted expression of *Nlrp3* in MCs, suggesting that LPS regulates inflammasome activation via several mechanisms in MCs. In macrophages, ATP-driven stimulation through the P2x7r is essential for caspase-1 proteolytic cleavage and IL-1β secretion via Nlrp3 (10, 19). The P2x7r forms a nonselective ion channel upon activation with ATP (19) and upon stimulation mediates K^+ efflux, which may be important for Nlrp3 activation (21). This ion channel mediated by P2x7r rapidly transitions to a pore-like structure by recruiting the pannexin-1 pore, which allows passage of molecules as large as 900 D (19). Therefore, it is possible, as it has been proposed for macrophages (37), that ATP promotes passage of microbial ligands such as LPS via pannexin-1 to trigger inflammasome activation in MCs. Consistently, ATP did not induce caspase-1 activation alone and triggered large pore formation in MCs, and this activity was blocked in P2x7r-deficient MCs. Unlike ATP, however, R837 did not induce large pore formation but elicited IL-1β secretion, at least in part, through P2x7r. The role of P2x7r in mediating IL-1β secretion in response to R837 stimulation is consistent with the observation that high K^+ extracellular medium blocked IL-1β secretion in MCs. Collectively, these results suggest that ATP and R837 may promote inflammasome activation via different mechanisms in MCs, although both stimuli require P2x7r and K^+ efflux for effective IL-1β secretion in MCs.

We observed a reduction in the amounts of TNF-α and IL-6 produced by MCs lacking *Nlrp3* compared with those from WT or Asc-deficient cells. The reason for this different regulation of cytokine secretion by Nlrp3 and Asc is unclear. One possibility is that Nlrp3 contributes to MC maturation in an Asc-independent manner. *Nlrp3* was first reported as an MC maturation–inducible gene (38) whose expression was

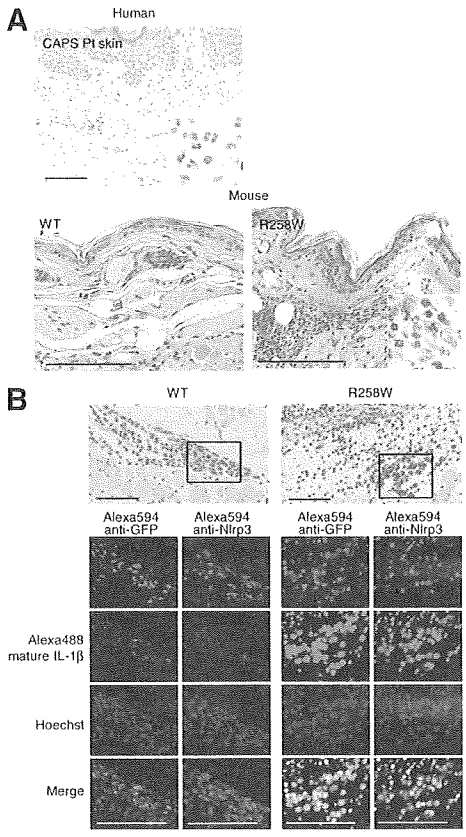

Figure 7. MCs expressing disease-associated Nlrp3 mutant induce neutrophil-rich inflammation in the mouse skin. 10^5 MC/9 cells expressing WT or mutant Nlrp3 (R258W) were injected into the skin of mice. (A, top) Representative images of the involved skin from a CAPS patient harboring an E567K *NLRP3* mutation. (bottom) Cross sections of mouse ears 36 h after injection with MC/9 cells. Tissue sections were stained with hematoxylin and eosin. Insets show a higher magnification demonstrating the presence of numerous neutrophils. Bars, 100 µm. (B) IL-1β expression in GFP^+ and $Nlrp3^+$ MC/9 cells. (bottom) Immunofluorescence images of mouse skin injected with MC/9 cells expressing WT or R258W-Nlrp3. Images were derived from tissues boxed in the top panels. All results are representative of at least three separate experiments. Bars, 50 µm.

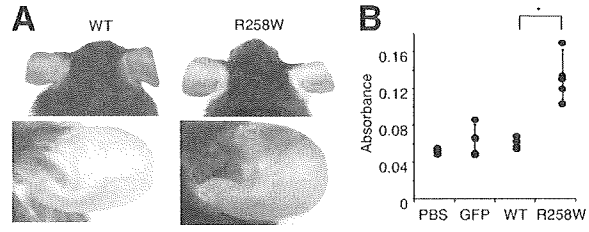

Figure 8. MCs expressing disease-associated Nlrp3 mutant induce vascular leakage in the mouse skin. Vascular leakage was analyzed by intravenous injection of 1% Evans blue solution 36 h after injection of mice with MC/9 cells expressing WT and mutant Nlrp3. (A, left) Mouse ears 30 min after dye injection. (B) Ears were collected, and vascular leakage was determined by absorbance at 620 nm in dye tissue extracts. Error bars represent means ± SD of results that are representative of at least three separate experiments. *, $P < 0.005$ between WT and R258W ($n = 4$ or 5 mice per group).

Published May 11, 2009

JEM

increased after the maturation into MCs with a connective tissue phenotype. Our BMCMCs were cultured with IL-3 and stem cell factor, which partially induce connective tissue–type maturation compared with the cells cultured with IL-3 alone. This possibility may explain, at least in part, why CAPS patients suffered from skin eruption but not asthma reaction or rhinitis, even though MCs in these tissues are likely to express the constitutively activated disease-associated NLRP3 mutation. However, no morphological and functional differences were observed between WT and Nlrp3-deficient MCs. Alternatively, Nlrp3 may directly or indirectly regulate cytokine production independently of the inflammasome in MCs.

CAPS-associated NLRP3 mutants constitutively produced IL-1β in MCs of the skin of patients and when injected into mouse tissues. However, it remains unclear why MCs with constitutive activation of the NLRP3 inflammasome produce mature IL-1β in the absence of LPS in patients given that microbial stimulation appears to be required for pro–IL-1β production. One possibility is that CAPS-associated NLRP3 mutants induce pro–IL-1β via constitutive activation of NF-κB induction, which is consistent with results found in the current work and also reported by others (26). Another possibility is that production of pro–IL-1β is induced by endogenous or environmental cues operating in the skin independently of NLRP3. Consistent with this model, the characteristic skin rash observed in CAPS and systemic inflammatory syndromes often develops within the first few weeks of life when the skin is first exposed to environmental factors. These may include exposure to small amounts of LPS and/or other microbial stimuli after birth. The observation that skin abnormalities in incontinentia pigmenti (MIM 308300), an X-linked dominant inherited disorder caused by the mutation of *NEMO*, a gene that encodes the regulatory component of the IκB kinase complex responsible for the activation of the NF-κB signaling pathway, commence at birth (39, 40) is also consistent with this possibility.

Urticarial rash associated with CAPS is usually nonpruritic and unresponsive to antihistamines. This clinical observation is in accordance with our observation that NLRP3 inflammasome activation induces IL-1β secretion but not degranulation in MCs. Nonetheless, MCs expressing CAPS-associated NLRP3 mutant promoted vascular permeability, a cellular response also induced by histamine release, which is critical for wheal formation in vivo. Because many cases of non-CAPS urticaria are unresponsive to histamine receptor antagonists, it is possible that skin rash associated with histamine resistance is mediated via inflammasome activation in MCs. Thus, understanding the pathophysiology of CAPS may provide critical insight into more common diseases such as antihistamine-refractory urticaria.

MATERIALS AND METHODS

Chemicals and reagents. Ultrapure LPS (*Escherichia coli* O55:B5), ATP, and MG-132 (Z-Leu-Leu-Leu-al) were purchased from Sigma-Aldrich. R837 (tlrl-imq) was purchased from InvivoGen. Abs for human cleaved IL-1β and IL-1β were purchased from Cell Signaling Technology, and human HLA-DR, -DP, -DQ (TAL.1B5) was purchased from Dako. Anti–human tryptase (G3) was provided by L. Schwartz (Virginia Commonwealth University, Richmond, VA). Anti–mouse IL-1β was purchased from R&D Systems. Abs for actin and cryopyrin were purchased from Santa Cruz Biotechnology, Inc., Tlr7 was purchased from Imgenex, and I-A^b (clone AF6-120.1) was purchased from BD. Anti-GFP was purchased from MBL International, and FITC- or Texas red–conjugated avidin was purchased from Invitrogen. Alexa Fluor 647–labeled anti–mouse IL-1β, Alexa Fluor 647–labeled anti-Ly-6G, and PE-labeled anti-CD45 were purchased from eBioscience.

Animals. *Nlrp3*$^{-/-}$, *Asc*$^{-/-}$, *Nlrc4*$^{-/-}$, and *P2x7r*$^{-/-}$ mice backcrossed at least eight times to C57BL6/J6 mice have been previously described (11, 41, 42). C57BL6/J6 mice were purchased from Crea Japan and housed in a pathogen-free facility. The animal studies were conducted under approved protocols by the Committee on the Use and Care of Animals of the University of Michigan and Chiba University.

Cultured MCs. The preparations of BMCMCs and FSMCs were previously described (24). The purity of MCs was confirmed by surface expression of CD45 and Kit, FITC-avidin labeling, and negative I-A^b expression (Fig. S2 A). Degranulation of MCs was assessed by β-hexosaminidase assay as previously described (24). Human MCs from cord blood were cultured as previously described (43).

Plasmid construction and retrovirus production. Plasmids to express mouse Nlrp3 have been previously described (31). Mutant Nlrp3 constructs corresponding to a human disease-associated mutation in the pEF-BOS vector were generated as previously described (18, 44). The ability of each construct to induce NF-κB activation was assessed with mouse Asc plasmid as previously described (18, 44). The retrovirus vector pMC-IRES-GFP (provided from T. Kitamura, University of Tokyo, Tokyo, Japan) containing Nlrp3 and its mutants was produced and introduced into Plat-E packaging cells with FuGENE6 (Roche). Immature BMCMCs cultured for 2 wk were incubated with retroviral supernatants for 15 h with 10 μg/ml polybrene (Sigma-Aldrich) (45). GFP-Nlrp3 fusion proteins were cloned into the pMX-IP vector and transfected into Plat-E cells. MC/9 cells were incubated with virus-containing supernatants and selected with 1.5 mg/ml puromycin.

Immunohistochemistry. Human and mouse skin biopsy samples were fixed with 4% paraformaldehyde, embedded in paraffin, and sectioned. Sections were stained with hematoxylin and eosin staining. Immunohistochemical staining was performed with primary Abs at the recommended concentrations followed by incubation with fluorescent dye–conjugated secondary Abs. Written informed consents were obtained from patients, according to the protocol of the institutional review board of Kyoto University Hospital and in accordance with the Declaration of Helsinki.

RT-PCR. Total RNA extracted from MCs (2×10^6) with TRIzol reagent (Invitrogen) was reverse transcribed and analyzed. The primers were as follows: *Nlrp3*, 5′-CACTTGGATCTAGCCACATC-3′ and 5′-AGCTCCAGCTTAAGGGAACTC-3′; *Asc*, 5′-ACTTGTCAGGGGATGAACTC-3′ and 5′-TGGTACTGTCCTTCAGTCAG-3′; *Casp1*, 5′-TACCTGGCAGGAATTCTGGA-3′ and 5′-ATGATCACCTTGGGCTTGTC-3′; *Il1b*, 5′-GCTTCCAAACCTTTGACCTG-3′ and 5′-CTGTTGTTTCCCAGGAAGAC-3′; *Tlr4*, 5′-CTGGCATCATCTTCATTGTCC-3′ and 5′-GCTTAGCAGCCATGTGTGTTCC-3′; *Tlr7*, 5′-CCACCAGACCTCTTGATTCC-3′ and 5′-TCCAGATGGTTCAGCCTACG-3′; *Gapdh*, 5′-CGGGAAGCTTGTCATCAATGG-3′ and 5′-GGCAGTGTGATGGCATGGATCTG-3′; *NLRP3*, 5′-AACAGCCACCTCACTTCCAG-3′ and 5′-GACGTAAGGCCAGAATTCAC-3′; *ASC*, 5′-TGGTCAGCTTCTACCTGGAG-3′ and 5′-TCCAGGCTGGTGTGAAACTG-3′; *CASP1*, 5′-GTACTTTCTTCCTTTCCAGCTC-3′ and 5′-TTCACATCTACGCTGTACCC-3′; and *IL1B*, 5′-TTCACATCTACGCTGTACCC-3′ and 5′-GTACTTTCTTCCTTTCCACCTC-3′. For real-time analysis, the mixture with Power SYBR Green PCR Master Mix (Applied Biosystems)

Published May 11, 2009

was amplified and analyzed with 7300 Real-Time PCR systems (Applied Biosystems).

Immunoblotting. Cell extracts were prepared in M-PER reagent (Thermo Fisher Scientific) in the presence of protease inhibitor cocktail (Thermo Fisher Scientific). Samples were denatured in 2× Laemmli sample buffer (Bio-Rad Laboratories) with 1 µl 2-ME. Lysates were separated by SDS-PAGE and transferred onto membranes (GE Healthcare). Membranes were incubated with an Ab against caspase-1, IL-1β, GFP, Tlr7, and actin, followed by horseradish peroxidase–conjugated Abs. Immunoreactive proteins were visualized with ECL detection reagents (GE Healthcare).

Cytokine ELISAs. Supernatants collected from 10^6 MCs/ml were measured for IL-1β (eBioscience), histamine (Invitrogen), TNF-α, and IL-6 (R&D Systems) by ELISA.

Neutrophil migration assay and histamine release. MC/9 cells stably expressing WT or mutant Nlrp3 (R258W) were suspended in PBS (10^7 cells/ml) and administrated i.p. (0.5 ml/mouse). 36 h after the injection, mice were sacrificed and the peritoneal cavity was lavaged with 2 ml PBS. After gentle massage, 1 ml of the peritoneal fluid was collected and centrifuged at 500 *g* for 5 min. Cells were stained for FACS analysis and the supernatant was used for histamine assay.

Evans blue dye injection assay. We modified the passive cutaneous anaphylaxis assay in mice as previously described (46). Right ears were injected intradermally with 10^5 cells in 0.1 ml saline and left ears were injected with saline as a control; 36 h later, mice were challenged with 0.5 ml saline containing 5 mg/ml Evans blue dye. Extravasation of Evans blue dye was monitored for 15 min, and ear biopsies were incubated at 63°C overnight in 700 µl formamide. Quantitative analysis of extracts was determined by measuring the absorbance at 620 nm.

Statistical analyses. All data are expressed as means ± SD. We accumulated the data for each condition from at least three independent experiments. We evaluated statistical significance with the Student's *t* test for comparisons between two mean values.

Online supplemental material. Fig. S1 shows the immunochemical staining of a CAPS patient's skin where tryptase-positive MCs, but not HLA-DR, -DP, -DQ–positive DCs or macrophages, were labeled with avidin and produced mature IL-1β. Fig. S2 shows the purity of BMCMCs and negative protein expression of Tlr7 on BMCMCs. Fig. S3 shows IL-1β, TNF-α, and IL-6 secretion from MCs in WT and Nlrc4-deficient mice. Fig. S4 shows a PCR analysis of the inflammasome components in mouse FSMCs that produced IL-1β, but did not show degranulation, in response to Nlrp3 activator. Fig. S5 shows a PCR analysis of the inflammasome components in human MCs that produced IL-1β in response to Nlrp3 activator. Fig. S6 shows the schematic structures of plasmids in pMX-IP retrovirus vector and the purity of MC/9 stably Nlrp3-GFP–expressing cells that did not show degranulation in response to Nlrp3 activator. Online supplemental material is available at http://www.jem.org/cgi/content/full/jem.20082179/DC1.

We would like to thank T. Kitamura for providing the pMC and pMX retrovirus system and Plat-E packaging cells, A. Fujisawa and H. Tanizaki for producing the plasmid for Nlrp3 disease-associated mutants, A. Niwa for help with human cord blood samples, S. Kagami and H. Umebayashi for the care of the patients, and G. Chen for critical review of the manuscript. We would also like to thank Y. Miyachi, T. Nakahata, and S. Shimada for encouragement and support of the work.

This work was supported in part by Grants-in-Aid for Scientific Research from the Ministry of Education, Culture, Sports, Science and Technology of Japan to N. Kambe (17790766 and 19591303), R. Nishikomori (19591249), M. Saito (195229), and H. Matsue (18390311 and 19659281), and grants from the National Institutes of Health (AI063331 and AR051790) to G. Núñez.

The authors have no conflicting financial interests.

Submitted: 29 September 2008
Accepted: 16 March 2009

REFERENCES

1. Nettis, E., A. Pannofino, C. D'Aprile, A. Ferrannini, and A. Tursi. 2003. Clinical and aetiological aspects in urticaria and angio-oedema. *Br. J. Dermatol.* 148:501–506.
2. Greaves, M. 2000. Chronic urticaria. *J. Allergy Clin. Immunol.* 105:664–672.
3. Sabroe, R.A., and M.W. Greaves. 2006. Chronic idiopathic urticaria with functional autoantibodies: 12 years on. *Br. J. Dermatol.* 154:813–819.
4. Kozel, M.M., and R.A. Sabroe. 2004. Chronic urticaria: aetiology, management and current and future treatment options. *Drugs.* 64:2515–2536.
5. Hull, K.M., N. Shoham, J.J. Chae, I. Aksentijevich, and D.L. Kastner. 2003. The expanding spectrum of systemic autoinflammatory disorders and their rheumatic manifestations. *Curr. Opin. Rheumatol.* 15:61–69.
6. Martinon, F., K. Burns, and J. Tschopp. 2002. The inflammasome: a molecular platform triggering activation of inflammatory caspases and processing of proIL-beta. *Mol. Cell.* 10:417–426.
7. Hoffman, H.M., J.L. Mueller, D.H. Broide, A.A. Wanderer, and R.D. Kolodner. 2001. Mutation of a new gene encoding a putative pyrin-like protein causes familial cold autoinflammatory syndrome and Muckle-Wells syndrome. *Nat. Genet.* 29:301–305.
8. Agostini, L., F. Martinon, K. Burns, M.F. McDermott, P.N. Hawkins, and J. Tschopp. 2004. NALP3 forms an IL-1beta-processing inflammasome with increased activity in Muckle-Wells autoinflammatory disorder. *Immunity.* 20:319–325.
9. Mariathasan, S., K. Newton, D.M. Monack, D. Vucic, D.M. French, W.P. Lee, M. Roose-Girma, S. Erickson, and V.M. Dixit. 2004. Differential activation of the inflammasome by caspase-1 adaptors ASC and Ipaf. *Nature.* 430:213–218.
10. Mariathasan, S., D.S. Weiss, K. Newton, J. McBride, K. O'Rourke, M. Roose-Girma, W.P. Lee, Y. Weinrauch, D.M. Monack, and V.M. Dixit. 2006. Cryopyrin activates the inflammasome in response to toxins and ATP. *Nature.* 440:228–232.
11. Kanneganti, T.D., N. Ozoren, M. Body-Malapel, A. Amer, J.H. Park, L. Franchi, J. Whitfield, W. Barchet, M. Colonna, P. Vandenabeele, et al. 2006. Bacterial RNA and small antiviral compounds activate caspase-1 through cryopyrin/Nalp3. *Nature.* 440:233–236.
12. Dostert, C., V. Petrilli, R. Van Bruggen, C. Steele, B.T. Mossman, and J. Tschopp. 2008. Innate immune activation through Nalp3 inflammasome sensing of asbestos and silica. *Science.* 320:674–677.
13. Eisenbarth, S.C., O.R. Colegio, W. O'Connor, F.S. Sutterwala, and R.A. Flavell. 2008. Crucial role for the Nalp3 inflammasome in the immunostimulatory properties of aluminium adjuvants. *Nature.* 453:1122–1126.
14. Li, H., S.B. Willingham, J.P. Ting, and F. Re. 2008. Cutting edge: inflammasome activation by alum and alum's adjuvant effect are mediated by NLRP3. *J. Immunol.* 181:17–21.
15. Saito, M., A. Fujisawa, R. Nishikomori, N. Kambe, M. Nakata-Hizume, M. Yoshimoto, K. Ohmori, I. Okafuji, T. Yoshioka, T. Kusunoki, et al. 2005. Somatic mosaicism of CIAS1 in a patient with chronic infantile neurologic, cutaneous, articular syndrome. *Arthritis Rheum.* 52:3579–3585.
16. Feldmann, J., A.M. Prieur, P. Quartier, P. Berquin, S. Certain, E. Cortis, D. Teillac-Hamel, A. Fischer, and G. de Saint Basile. 2002. Chronic infantile neurological cutaneous and articular syndrome is caused by mutations in CIAS1, a gene highly expressed in polymorphonuclear cells and chondrocytes. *Am. J. Hum. Genet.* 71:198–203.
17. Manji, G.A., L. Wang, B.J. Geddes, M. Brown, S. Merriam, A. Al-Garawi, S. Mak, J.M. Lora, M. Briskin, M. Jurman, et al. 2002. PYPAF1, a PYRIN-containing Apaf1-like protein that assembles with ASC and regulates activation of NF-kappa B. *J. Biol. Chem.* 277:11570–11575.
18. Saito, M., R. Nishikomori, N. Kambe, A. Fujisawa, H. Tanizaki, K. Takeichi, T. Imagawa, T. Iehara, H. Takada, T. Matsubayashi, et al. 2008. Disease-associated CIAS1 mutations induce monocyte death, revealing low-level mosaicism in mutation-negative cryopyrin-associated periodic syndrome patients. *Blood.* 111:2132–2141.
19. Ferrari, D., C. Pizzirani, E. Adinolfi, R.M. Lemoli, A. Curti, M. Idzko, E. Panther, and F. Di Virgilio. 2006. The P2X7 receptor: a key player in IL-1 processing and release. *J. Immunol.* 176:3877–3883.
20. Bulanova, E., V. Budagian, Z. Orinska, M. Hein, F. Petersen, L. Thon, D. Adam, and S. Bulfone-Paus. 2005. Extracellular ATP induces cytokine expression and apoptosis through P2X7 receptor in murine mast cells. *J. Immunol.* 174:3880–3890.

Published May 11, 2009

JEM

21. Pelegrin, P., and A. Surprenant. 2006. Pannexin-1 mediates large pore formation and interleukin-1beta release by the ATP-gated P2X7 receptor. *EMBO J.* 25:5071–5082.
22. Amer, A., L. Franchi, T.D. Kanneganti, M. Body-Malapel, N. Ozoren, G. Brady, S. Meshinchi, R. Jagirdar, A. Gewirtz, S. Akira, and G. Nunez. 2006. Regulation of *Legionella* phagosome maturation and infection through flagellin and host Ipaf. *J. Biol. Chem.* 281:35217–35223.
23. Franchi, L., A. Amer, M. Body-Malapel, T.D. Kanneganti, N. Ozoren, R. Jagirdar, N. Inohara, P. Vandenabeele, J. Bertin, A. Coyle, et al. 2006. Cytosolic flagellin requires Ipaf for activation of caspase-1 and interleukin 1beta in salmonella-infected macrophages. *Nat. Immunol.* 7:576–582.
24. Yamada, N., H. Matsushima, Y. Tagaya, S. Shimada, and S.I. Katz. 2003. Generation of a large number of connective tissue type mast cells by culture of murine fetal skin cells. *J. Invest. Dermatol.* 121:1425–1432.
25. Piccini, A., S. Carta, S. Tassi, D. Lasiglie, G. Fossati, and A. Rubartelli. 2008. ATP is released by monocytes stimulated with pathogen-sensing receptor ligands and induces IL-1beta and IL-18 secretion in an autocrine way. *Proc. Natl. Acad. Sci. USA.* 105:8067–8072.
26. Dowds, T.A., J. Masumoto, L. Zhu, N. Inohara, and G. Nunez. 2004. Cryopyrin-induced interleukin 1beta secretion in monocytic cells: enhanced activity of disease-associated mutants and requirement for ASC. *J. Biol. Chem.* 279:21924–21928.
27. Kagami, S., H. Saeki, Y. Kuwano, S. Imakado, and K. Tamaki. 2006. A probable case of Muckle-Wells syndrome. *J. Dermatol.* 33:118–121.
28. Galli, S.J., M. Grimbaldeston, and M. Tsai. 2008. Immunomodulatory mast cells: negative, as well as positive, regulators of immunity. *Nat. Rev. Immunol.* 8:478–486.
29. Supajatura, V., H. Ushio, A. Nakao, S. Akira, K. Okumura, C. Ra, and H. Ogawa. 2002. Differential responses of mast cell Toll-like receptors 2 and 4 in allergy and innate immunity. *J. Clin. Invest.* 109:1351–1359.
30. Lin, T.J., R. Garduno, R.T. Boudreau, and A.C. Issekutz. 2002. *Pseudomonas aeruginosa* activates human mast cells to induce neutrophil transendothelial migration via mast cell-derived IL-1 alpha and beta. *J. Immunol.* 169:4522–4530.
31. Hoffman, H.M., S. Rosengren, D.L. Boyle, J.Y. Cho, J. Nayar, J.L. Mueller, J.P. Anderson, A.A. Wanderer, and G.S. Firestein. 2004. Prevention of cold-associated acute inflammation in familial cold autoinflammatory syndrome by interleukin-1 receptor antagonist. *Lancet.* 364:1779–1785.
32. Nigrovic, P.A., B.A. Binstadt, P.A. Monach, A. Johnsen, M. Gurish, Y. Iwakura, C. Benoist, D. Mathis, and D.M. Lee. 2007. Mast cells contribute to initiation of autoantibody-mediated arthritis via IL-1. *Proc. Natl. Acad. Sci. USA.* 104:2325–2330.
33. Dietsch, G.N., and D.J. Hinrichs. 1989. The role of mast cells in the elicitation of experimental allergic encephalomyelitis. *J. Immunol.* 142:1476–1481.
34. Robbie-Ryan, M., M.B. Tanzola, V.H. Secor, and M.A. Brown. 2003. Cutting edge: both activating and inhibitory Fc receptors expressed on mast cells regulate experimental allergic encephalomyelitis disease severity. *J. Immunol.* 170:1630–1634.
35. Tanzola, M.B., M. Robbie-Ryan, C.A. Gutekunst, and M.A. Brown. 2003. Mast cells exert effects outside the central nervous system to influence experimental allergic encephalomyelitis disease course. *J. Immunol.* 171:4385–4391.
36. Neven, B., A.M. Prieur, and P. Quartier dit Maire. 2008. Cryopyrinopathies: update on pathogenesis and treatment. *Nat. Clin. Pract. Rheumatol.* 4:481–489.
37. Kanneganti, T.D., M. Lamkanfi, Y.G. Kim, G. Chen, J.H. Park, L. Franchi, P. Vandenabeele, and G. Nunez. 2007. Pannexin-1-mediated recognition of bacterial molecules activates the cryopyrin inflammasome independent of Toll-like receptor signaling. *Immunity.* 26:433–443.
38. Kikuchi-Yanoshita, R., Y. Taketomi, K. Koga, T. Sugiki, Y. Atsumi, T. Saito, S. Ishii, M. Hisada, T. Suzuki-Nishimura, M.K. Uchida, et al. 2003. Induction of PYPAF1 during in vitro maturation of mouse mast cells. *J. Biochem.* 134:699–709.
39. Berlin, A.L., A.S. Paller, and L.S. Chan. 2002. Incontinentia pigmenti: a review and update on the molecular basis of pathophysiology. *J. Am. Acad. Dermatol.* 47:169–187.
40. Nelson, D.L. 2006. NEMO, NFkappaB signaling and incontinentia pigmenti. *Curr. Opin. Genet. Dev.* 16:282–288.
41. Kanneganti, T.D., M. Body-Malapel, A. Amer, J.H. Park, J. Whitfield, L. Franchi, Z.F. Taraporewala, D. Miller, J.T. Patton, N. Inohara, and G. Nunez. 2006. Critical role for Cryopyrin/Nalp3 in activation of caspase-1 in response to viral infection and double-stranded RNA. *J. Biol. Chem.* 281:36560–36568.
42. Ozoren, N., J. Masumoto, L. Franchi, T.D. Kanneganti, M. Body-Malapel, I. Erturk, R. Jagirdar, L. Zhu, N. Inohara, J. Bertin, et al. 2006. Distinct roles of TLR2 and the adaptor ASC in IL-1beta/IL-18 secretion in response to *Listeria monocytogenes*. *J. Immunol.* 176:4337–4342.
43. Kambe, N., H. Hiramatsu, M. Shimonaka, H. Fujino, R. Nishikomori, T. Heike, M. Ito, K. Kobayashi, Y. Ueyama, N. Matsuyoshi, et al. 2004. Development of both human connective tissue-type and mucosal-type mast cells in mice from hematopoietic stem cells with identical distribution pattern to human body. *Blood.* 103:860–867.
44. Fujisawa, A., N. Kambe, M. Saito, R. Nishikomori, H. Tanizaki, N. Kanazawa, S. Adachi, T. Heike, J. Sagara, T. Suda, et al. 2007. Disease-associated mutations in CIAS1 induce cathepsin B-dependent rapid cell death of human THP-1 monocytic cells. *Blood.* 109:2903–2911.
45. Nishiyama, C., M. Nishiyama, T. Ito, S. Masaki, K. Maeda, N. Masuoka, H. Yamane, T. Kitamura, H. Ogawa, and K. Okumura. 2004. Overproduction of PU.1 in mast cell progenitors: its effect on monocyte- and mast cell-specific gene expression. *Biochem. Biophys. Res. Commun.* 313:516–521.
46. Kabu, K., S. Yamasaki, D. Kamimura, Y. Ito, A. Hasegawa, E. Sato, H. Kitamura, K. Nishida, and T. Hirano. 2006. Zinc is required for Fc epsilon RI-mediated mast cell activation. *J. Immunol.* 177:1296–1305.
47. Duncan, J.A., D.T. Bergstralh, Y. Wang, S.B. Willingham, Z. Ye, A.G. Zimmermann, and J.P. Ting. 2007. Cryopyrin/NALP3 binds ATP/dATP, is an ATPase, and requires ATP binding to mediate inflammatory signaling. *Proc. Natl. Acad. Sci. USA.* 104:8041–8046.

Stepwise differentiation of pluripotent stem cells into retinal cells

Fumitaka Osakada[1,2], Hanako Ikeda[1–3], Yoshiki Sasai[2] & Masayo Takahashi[1]

[1]Laboratory for Retinal Regeneration, Center for Developmental Biology, RIKEN, Kobe, Japan. [2]Organogenesis and Neurogenesis Group, Center for Developmental Biology, RIKEN, Kobe, Japan. [3]Shiga Medical Center for Adults, Shiga, Japan. Correspondence should be addressed to F.O. (osakada@cdb.riken.jp).

Published online 7 May 2009; doi:10.1038/nprot.2009.51

Embryonic stem (ES) cells are pluripotent cells derived from the inner cell mass of blastocyst-stage embryos. They can maintain an undifferentiated state indefinitely and can differentiate into derivatives of all three germ layers, namely ectoderm, endoderm and mesoderm. Although much progress has been made in the propagation and differentiation of ES cells, induction of photoreceptors has generally required coculture with or transplantation into developing retinal tissue. Here, we describe a protocol for generating retinal cells from ES cells by stepwise treatment with defined factors. This method preferentially induces photoreceptor and retinal pigment epithelium (RPE) cells from mouse and human ES cells. In our protocol, differentiation of RPE and photoreceptors from mouse ES cells requires 28 d and the differentiation of human ES cells into mature RPE and photoreceptors requires 120 and 150 d, respectively. This differentiation system and the resulting pluripotent stem cell-derived retinal cells will facilitate the development of transplantation therapies for retinal diseases, drug testing and *in vitro* disease modeling. It will also improve our understanding of the development of the central nervous system, especially the eye.

INTRODUCTION

Embryonic stem cells are pluripotent cells derived from the inner cell mass of blastocyst-stage embryos. They can grow indefinitely and can differentiate into derivatives of all three germ layers, namely ectoderm, endoderm and mesoderm[1]. These properties make ES cells powerful tools for modeling development and disease, as well as for developing cell replacement therapies. As functional impairment results from cell loss in most central nervous system (CNS) diseases, recovery of lost cells is an important treatment strategy. Neurogenesis occurs in two regions of the adult mammalian brain[2]. In the adult retina, Müller glia serve as endogenous retinal progenitors in response to injury[3,4] (**Fig. 1a,b**). However, the CNS has poor potential for regeneration to compensate for cell loss. Thus, transplantation of ES cell-derived neurons into damaged or diseased CNS is a promising treatment approach for neurodegenerative disorders, including Parkinson's disease, Huntington's disease, spinal cord injury and stroke[5].

Most retinal degeneration diseases in humans are caused by the impairment of the neural retina, which causes irreversible blindness. For instance, in retinitis pigmentosa, photoreceptors are selectively lost owing to genetic mutations[6]. In age-related macular degeneration, degeneration of the RPE is followed by the loss of photoreceptors[7]. Thus, transplantation of photoreceptor or RPE cells may permit recovery of visual function.

Accumulating evidence indicates that RPE cells derived from monkey and human ES cells can restore visual function in a retinal degeneration model, the Royal College of Surgeons (RCS) rat[8,9]. On postnatal days (P) 3–6, postmitotic rod photoreceptors are able to form functional synaptic connections with host bipolar cells and to improve visual function when transplanted into the normal or degenerating adult mouse retina[10]. It is of note that the stage of differentiation of donor photoreceptors is important for successful transplantation. As somatic progenitors derived from the adult ciliary body[11] or the iris[12] are limited in both differentiation potential and proliferation capacity (**Fig. 1a,c**), ES cells and induced pluripotent stem cells[13–15] represent a promising donor source for transplantation, if indeed P3–6 photoreceptors can be induced from them. A reliable and efficient *in vitro* method of

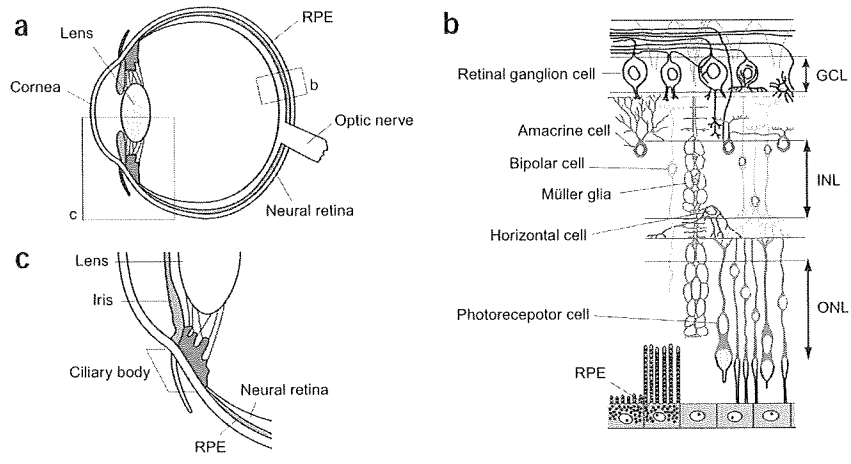

Figure 1 | Localization of neural stem/progenitor cells in adult eye tissue. Schematic diagram of a section of an adult mammalian eye (**a**). Magnified views of boxed region in panel **a** (b and c). Müller glia act as retinal progenitors in response to injury (**b**, purple). Retinal progenitors are present in the ciliary body (**a,c**: red). Iris-derived cells display neural stem/progenitor cell properties (**a,c**: orange). RPE, retinal pigment epithelium; GCL, ganglion cell layer; INL, inner nuclear layer; ONL, outer nuclear layer. (Reproduced with permission from ref. 23)

generating retinal cells from ES cells will greatly contribute to medical and pharmaceutical research aimed at finding treatments for retinal diseases[16–18].

In vitro differentiation of ES cells mimics, at least in part, the patterning and differentiation events that occur during embryogenesis[19–21]. During development of the neural plate, the anterior neurepithelium evaginates to give rise to the optic vesicle, then invaginates along with the overlying surface ectoderm to form a bilayered optic cup[22,23]. The outer layer of the optic cup differentiates into the RPE, whereas the inner neurepithelial layer differentiates into the neural retina. Within the neural retina, seven types of cells differentiate from a common set of progenitors in the following temporal sequence: retinal ganglion cells, cone photoreceptors, amacrine cells, horizontal cells, rod photoreceptors, bipolar cells and Müller glia[24]. As is the case for *in vivo* development, ES cells differentiate into retinal progenitors in response to patterning signals and subsequently differentiate into retinal cells in a stepwise fashion (**Fig. 2**). It is of note that ES cells have never been observed to differentiate directly into retinal cells[25,26].

Since the establishment of mouse ES cells in 1981 (see ref. 1) and human ES cells in 1998 (see ref. 27), much progress has been made in ES cell propagation and differentiation techniques. Over the last decade, several methods have been reported to control the differentiation of ES cells into neural cells[19,21,28–33]. Each method has its own advantages and disadvantages, depending on the type of neural cells desired, and can induce differentiation of neural tissues with distinct regional identities within the CNS[19–21]. ES cells can be differentiated into floating aggregates known as embryoid bodies, which are cultured in the presence of serum and contain cells derived from all three germ layers. In contrast, our method is based on a serum-free, feeder-free suspension culture, which can induce selective differentiation toward the ectoderm[21].

RPE cells can be generated from primate ES cells cocultured with PA6 stromal cells[34] and from human ES cells after spontaneous differentiation at a low efficiency with $<1\%$ of the embryoid bodies containing pigmented cells[35]. Retinal progenitors can also be generated from ES cells *in vitro*, but they rarely differentiate into photoreceptors unless cocultured with or transplanted into developing retinal tissues[36–38]. Factors involved in *in vivo* retinal development are critical for the *in vitro* differentiation of ES cells into retinal cells. On the basis of our knowledge of embryonic development, we have established a defined culture method for generating photoreceptors and RPE from mouse and human ES cells *in vitro*[25,26] (**Fig. 3**). This differentiation system and the resulting human ES cell-derived cells will substantially facilitate the development of human ES cell-based transplantation therapies for retinal diseases, the discovery of therapeutic drugs and the investigation of CNS development and disease mechanisms[39]. In addition, induced pluripotent stem cell technology will likely allow us to make progress on *in vitro* modeling and patient-specific therapy[40–42]. Here, we introduce our step-by-step protocol for inducing retinal progenitors, RPE cells and photoreceptors *in vitro* (**Figs. 2** and **3**).

Although the ES cell-derived photoreceptors we describe here express all the appropriate markers, we have not yet determined whether they can function normally. The function of photoreceptors has generally been tested by electrophysiology in retinal cells freshly prepared from animals, because the crucial outer segment of the cell is lost during cell culture. Thus, to test whether ES cell-derived photoreceptors are functional, we must transplant them into the developing and adult retina and analyze their function within retinal tissue. Transplantation studies will require large numbers of differentiated retinal cells. Although retinal cells can be obtained from mouse and human ES cells, the differentiation efficiency is low. The pluripotency of ES cells permits the use of large numbers of undifferentiated ES cells, but improvement of the differentiation efficiency is important for *in vitro* modeling of development and disease, drug screening and transplantation studies.

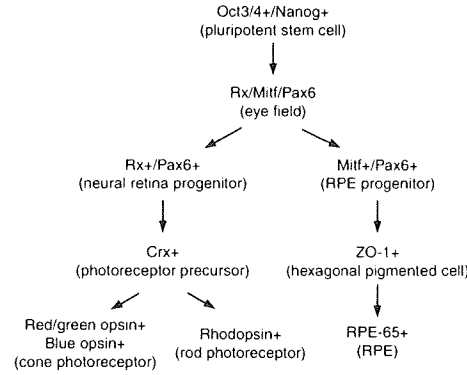

Figure 2 | Multistep commitment in the development of retinal cells. Markers for the differentiation steps are shown in bold font. ES cells differentiate into retinal cells in a stepwise manner along the developmental time course.

Experimental design

Mouse ES cells. Mouse ES cells should be passaged before reaching confluence (**Fig. 4a**), because overconfluent ES cells differentiate even under conditions that normally maintain pluripotency. We use mouse ES cells carrying a blasticidin-S resistance gene in the

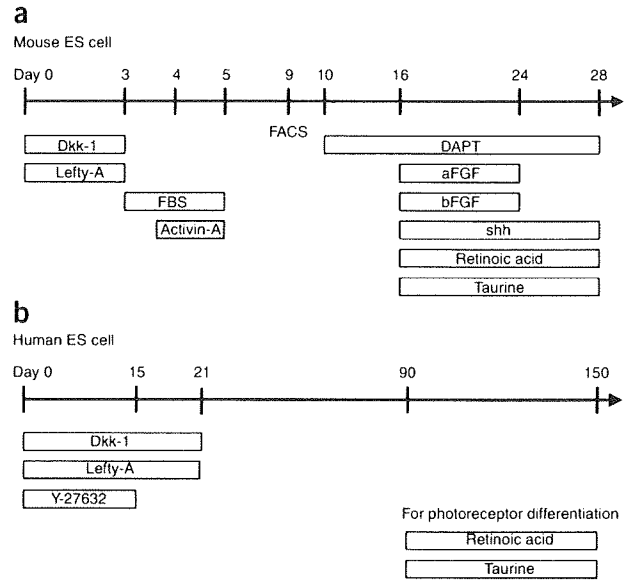

Figure 3 | Schematic diagram of mouse and human ES cell differentiation into retinal cells. Differentiation of mouse ES cells into retinal cells (**a**). Differentiation of human ES cells into retinal cells (**b**).

Oct-3/4 locus to select Oct-3/4+ undifferentiated pluripotent cells (**Fig. 4a**). Our mouse ES cells also contain a green fluorescent protein (GFP) reporter gene knocked into the Rx locus to aid in later purification[26]. To induce differentiation of mouse ES cells, we dissociate undifferentiated ES cell colonies into single cells and plate the cell suspension onto a Petri dish as a floating culture. Floating mouse ES cells spontaneously form aggregates within 1 d under these conditions (**Fig. 4b,c**). As shown in **Figure 3a**, we add Dkk-1, Lefty-A, fetal bovine serum (FBS) and Activin-A to the media to induce retinal specification of ES cells[25,26]. After the addition of Dkk-1 and Lefty-A on differentiation day 0, we replace half of the media with the media that do not contain Dkk-1 and Lefty-A on day 3. Thus, during days 3–5, Dkk-1 and Lefty-A are present at half concentration. We confirmed that the differentiation efficiency is the same at half concentration as at full concentration. Therefore, we have modified the earlier reported protocol. After the addition of FBS on day 3, cell aggregates become adherent. Thus, to avoid adhesion of floating cells to the culture dish, we re-plate the cell aggregates onto a 2-methacryloyloxyethyl phosphorylcholine (MPC)-treated non-adhesive dish. As the cells form aggregates, it is difficult to judge by cell morphology alone whether the protocol is carried out well. Thus, retinal marker expression should be examined by immunostaining or reverse transcriptase-PCR analysis. The transcription factor Rx plays an essential role in the specification of the retinal primordium and is an early marker of the eye field (**Fig. 2**). Rx-GFP expression peaks on differentiation day 9 and thereafter declines. Thus, we purify retinal progenitors using fluorescent-activated cell sorting (FACS) on day 9 (**Fig. 4d**). Without FACS, multiple cell types are present after differentiation, which may mask patterning signals for retinal specification. After FACS, we steer purified cells toward mature retinal phenotypes by modifying the reaggregation pellet culture reported by Watanabe and Raff[43] (**Fig. 5a**). *N*-[*N*-(3,5-Difluorophenacetyl)-L-alanyl]-*S*-phenylglycine *t*-butyl ester (DAPT) is added to increase the number of Crx+ photoreceptor precursors (**Fig. 2**), then fibroblast growth factors (FGFs), Sonic hedgehog N-terminal peptide (Shh), retinoic acid (RA) and taurine are added to promote rod differentiation, because these factors promote rod genesis from retinal progenitors *in vitro*[26,44] (**Figs. 5a–c** and **6a,b**). After addition of these factors, marked morphological changes are not observed immediately, as differentiation progresses slowly. We recommend monitoring differentiation by examining the expression of differentiation markers observed during eye development (**Figs. 2** and **6**) at various steps rather than by microscopy alone.

Human ES cells. Human ES cells require more careful handling compared with mouse ES cells. For instance, although mouse ES cells can be dissociated into single cells, a similar treatment of human ES cells causes cell death and abnormal karyotypes. We follow the method described by Suemori *et al.*[45] and maintain

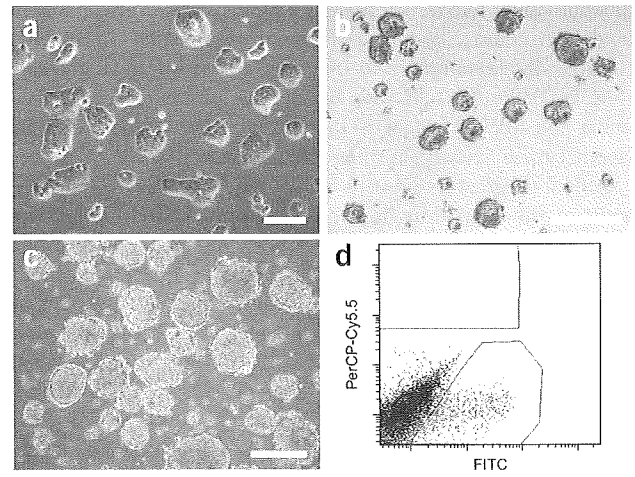

Figure 4 | Undifferentiated mouse ES cells, formed aggregates and FACS analysis. Typical morphology of undifferentiated mouse ES cell colonies cultured under feeder-free conditions (**a**). The shape of formed aggregates after 3 d (**b**) and 8 d (**c**) in the SFEB/DLFA culture. Typical data for FACS analysis (**d**). Rx-GFP+ mouse ES cells (green) are selected by flow cytometry. Scale bars, 300 μm.

human ES cells at 37 °C in a humidified atmosphere of 2% CO_2 and 98% air and use a mild enzymatic technique that enables bulk passaging of human ES cells and retention of normal karyotypes after more than 100 passages (**Fig. 7**). In addition, to improve cell survival during differentiation, the Rho kinase inhibitor, Y-27632, is added 1 h before dissociation and is maintained in the culture media during the first 15 days of floating culture, because Y-27632 prevents dissociation-induced cell death in human ES cells[46]. In our protocol for differentiation, ES cell colonies are dissociated into 5–10 cells per clump. It should be noted that efficiency of neural induction is low if ES clumps are too large. Furthermore, to avoid cell damage by centrifugation, we permit large aggregates to sink down to the bottom of the tube by gravity and use centrifugation only with small aggregates.

Unlike mouse ES cells, human ES cells require mouse embryonic fibroblast (MEF) feeder layers for maintenance. To prevent contamination with MEFs, we plate the cell suspension containing both human ES cells and MEFs onto gelatin-coated dishes before differentiation. MEFs adhere more quickly than do human ES cells, so incubating the dish for 1 h allows MEFs to adhere to the dish, while ES cells remain floating. To establish defined conditions for human ES cell culture, FBS is not used. For differentiation (**Fig. 3b**), human ES cells are incubated in the presence of Dkk-1 and Lefty-A for 21 d in a floating culture (**Fig. 8**) and are plated onto a fibronectin-, laminin- and poly-D-lysine-coated dish[26], which supports adhesion of cell aggregates and subsequent neural

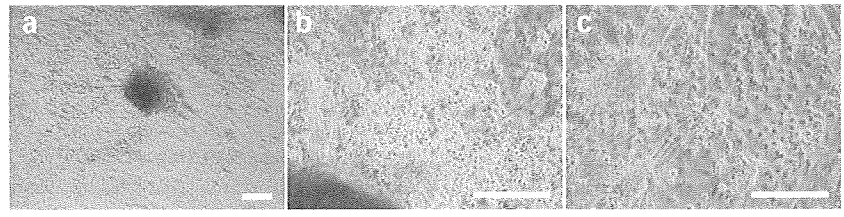

Figure 5 | Morphology of differentiated pelleted mouse ES cells after sorting. After FACS sorting and pellet formation, differentiated cells migrate out from the pellet in a radial manner (**a**). Round cells tend to be observed around the pellet (**b**). Neural- and epithelial-like cells tend to be observed far from the pellet (**c**). Scale bars, 100 μm.

differentiation. Excessively high plating density is not suitable for long-term culture, because cell growth is impeded. In adherent culture, differentiating cells migrate out from the aggregates (**Fig. 9**). Although cells with neurite-like processes are observed under the microscope, it is difficult to judge without staining whether these neural cells differentiate into retinal cells.

Retinal progenitors positive for Rx, Mitf and Pax6 are induced between differentiation days 30–40. Approximately 40 d after differentiation, pigmented cells can be observed under a light microscope. At this time, pigmented cells rarely have a polygonal shape, but long-term culture (>60 d) results in increased pigmentation and polygonal morphology (**Figs. 10** and **11**). Finally, treatment with RA and taurine, both of which are important for photoreceptor genesis, induces photoreceptor differentiation (**Figs. 12** and **13**).

Our method preferentially induces the differentiation of RPE and photoreceptors from ES cells. When the procedure is carried out smoothly, we observe pigmented colonies without having to perform any cell staining, unless the ES cells are derived from albino mice. Retinal cells differentiate only from colonies committed to retinal fate, whereas colonies not committed to the retinal fate fail to generate retinal cells, including pigmented cells. Thus, if pigmented cells are observed, other types of differentiated retinal cells should also be present.

Mouse and human ES cells differ in both their maintenance and differentiation conditions. Mouse ES cells can be maintained in a pluripotent state without a feeder layer when grown in the presence of LIF. In contrast, human ES cells require a feeder layer and addition of the growth factor, FGF-2, but not LIF. The condition of the MEF feeder layer is very important for maintaining undifferentiated human ES cells, and the preparation of MEF feeders is described in **Box 1**. Only early passage MEFs (up to passage 2) should be used to prepare feeders for human ES cell culture, and feeders should be used within 3 d of preparation.

Mouse ES cells can be genetically engineered more easily than human ES cells. We use mouse ES cells carrying internal ribosome entry site (IRES)-blasticidin-S deaminase in the Oct-3/4 locus, which allows for the selection of Oct-3/4+ undifferentiated pluripotent cells[26,47]. Purification methods must be devised to isolate target cells for transplantation, to prevent tumorigenesis resulting from undifferentiated ES cells, to establish *in vitro* models of development and disease and to facilitate drug screening[39,48]. To purify retinal progenitors, our mouse ES cells also contain a GFP reporter gene knocked into the Rx locus[26].

Differentiation of human ES cells takes a longer duration than that of mouse ES cells. Differentiation of mouse ES cells into RPE and photoreceptors requires ~1 month, whereas generation of mature RPE from human ES cells takes ~4 months, and photoreceptors require ~5 months. Even after 2 weeks of human ES cell differentiation, a small number of cells still express the undifferentiated ES cell markers, Oct3/4 and Nanog. It is possible that this difference in differentiation time between human and mouse ES cells is because of the large difference in time required for overall embryonic development. Further improvements to the differentiation protocol might enable faster generation of retinal cells from human ES cells.

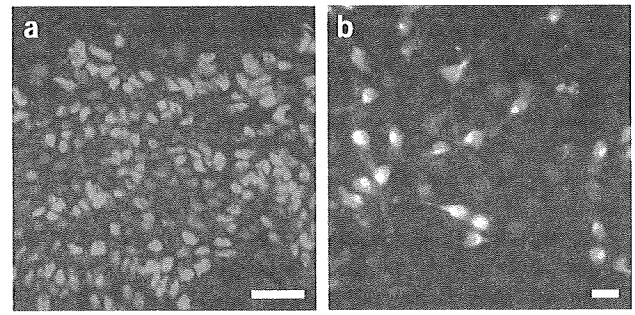

Figure 6 | Immunocytochemical analyses of the differentiated cells from mouse ES cells. The sorted Rx-GFP+ cells treated with DAPT express Crx on day 20 (**a**). The sorted cells treated with DAPT, aFGF, bFGF, shh, taurine and RA express rhodopsin and recoverin on day 28 (**b**). Scale bar, 20 μm (**a**) and 10 μm (**b**). (Reproduced with permission from ref. 26.)

Evaluation of ES cell differentiation. Evaluating the effectiveness of retinal differentiation can be performed using FACS analysis to quantify the differentiated cells. Knock-in ES cells expressing a fluorescent protein under the control of a specific promoter and antibody detection of specific cell surface antigens are both useful for FACS. Moreover, differentiation can be evaluated by immunocytochemistry. Antibodies that we have tested by staining appropriate tissues (frozen sections of embryonic, postnatal and adult eyes) are shown in **Table 1**. ES cells express the undifferentiated cell markers, Oct3/4, Nanog, TRA-1-60 and TRA-1-81 (**Fig. 2**). Staining for Rx, Mitf, Pax6 or Chx10 individually does not provide a good index for retinal differentiation, because these markers are also expressed in other CNS regions. For example, Rx is also expressed in the ventral diencephalon, Pax6 in the telencephalon and Mitf in melanocytes. However, co-immunostaining for Rx, Mitf, Pax6 and Chx10 in combination marks cells that have undergone retinal specification (**Fig. 2**). Quantitative PCR analysis can be used not only to examine the expression of markers for retinal differentiation but also to detect genes normally expressed in a specific developing brain region along the rostral–caudal and dorsal–ventral axes. This provides us with positional information of differentiated cells[20,21,33]. Finally, although analysis of human embryos is not possible because of ethical concerns, analysis of mouse embryonic development will help us learn molecular

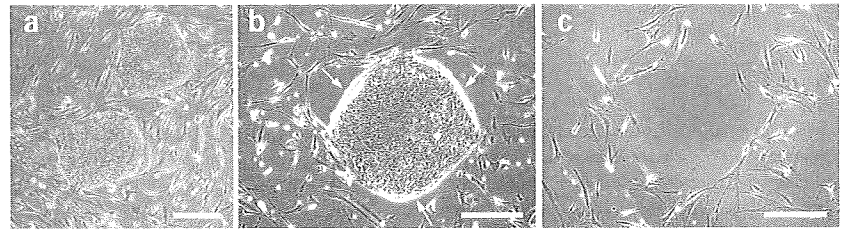

Figure 7 | Morphology of undifferentiated human ES cells and detachment of ES cell colonies. Typical morphology of undifferentiated human ES cell colonies cultured on MEF feeders (**a**). ES cell colonies have partially detached from the substratum (**b**). Arrows indicate the detached edge of human ES cell colonies. Human ES cell colonies are preferentially detached, whereas MEF feeders remain on the dish (**c**). Scale bar, 500 μm (**a**) and 300 μm (**b**,**c**).

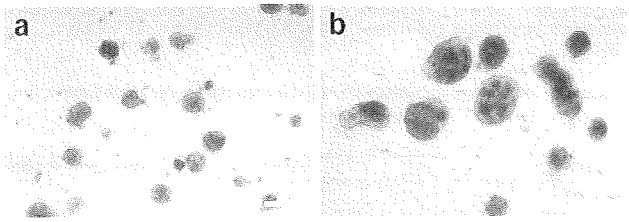

Figure 8 | Morphology of floating aggregates formed from human ES cells. The shape of aggregates formed after 6 d of culture (**a**) or 21 d of culture (**b**) in the SFEB/DLFA culture. Scale bars, 300 μm.

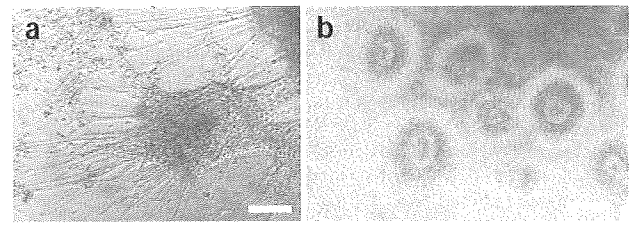

Figure 9 | Morphology of human ES cell aggregates in adherent culture. In adherent culture on day 30, differentiated cells extend from the aggregates in a radial manner (**a**). Neurite formation is observed (**a**). Some of the aggregates form neural rosettes on day 30 (**b**). Scale bars, 100 μm.

and cellular controls in the differentiation of ES cells toward various types of cells.

The variability of Knockout Serum Replacement (KSR) and FBS from one lot to another is a factor that affects the maintenance and differentiation of ES cells. For instance, a suboptimal lot of KSR or FBS can decrease the speed of colony growth and cause colony collapse and the loss of undifferentiated marker expression during maintenance. It can also inhibit neural or retinal differentiation. Therefore, we always test several lots of KSR and FBS on ES cells and measure the expression of various markers of differentiation by immunocytochemistry, reverse transcriptase-PCR or FACS analysis.

MATERIALS

REAGENTS

- Mouse ES cell: Rx-KI ES cell lines 116-18 and 20-10 (see refs. 26,47)
- Human ES cell: khES-1, khES-2 and khES-3 (see ref. 45)
- MEF (Kitayama Rabesu, cat. no. KBL9284600)
- Glasgow MEM (GMEM) (GIBCO, cat. no. 11710-035)
- DMEM/F12 (Sigma, cat. no. D6421)
- DMEM (Sigma, cat. no. D5796)
- KSR (GIBCO, cat. no. 10828-028)
- FBS (JRH Biosciences, cat. no. 12103-78P), heat-inactivated at 56 C for 30 min
- Minimum essential media Eagle, HEPES modification (Sigma, cat. no. M7278)
- Hank's balanced salt solution (GIBCO, cat. no. 24020-117)
- PBS (GIBCO, cat. no. 10010-023)
- dH_2O (GIBCO, cat. no. 15230-162)
- Dimethylsulfoxide (DMSO) (Nacalai, cat. no. 13408-64)
- Gelatin Type A (Sigma, cat. no. G2500) for mouse ES cells
- Gelatin Type B (Sigma, cat. no. G9391) for human ES cells
- Non-essential amino acid solution (Sigma, cat. no. M7145)
- Pyruvate, 100 mM solution (Sigma, cat. no. S8636)
- 2-Mercaptoethanol (2-ME) (Sigma, cat. no. M7522) ! **CAUTION** 2-ME is toxic. When used, avoid inhalation and skin contact.
- N2 supplement (GIBCO, cat. no. 17502-048)
- Glucose (Nacalai, cat. no. 16805-35)
- L-Glutamine (Sigma, cat. no. G7513)
- Penicillin/streptomycin (GIBCO, cat. no. 15070-063)
- 0.25% Trypsin–EDTA (GIBCO, cat. no. 25200-056)
- 2.5% (wt/vol) Trypsin (GIBCO, cat. no. 15090-046)
- Collagenase type IV (GIBCO, cat. no. 17104-019)
- Trypan blue stain (GIBCO, cat. no. 1520-061)
- Propidium iodide (PI) (Sigma, cat. no. P4170)
- Bovine serum albumin (BSA) (Sigma, cat. no. A2058)
- Blasticidin (Blas) (Funakoshi, cat. no. KK-400)
- LIF (ESGRO) (Chemicon, cat. no. R-ESG1107)
- Mitomycin C (Wako, cat. no. 134-07911)
- Dkk-1 (R&D Systems, cat. no. 1096-DK-010)
- Lefty-A (R&D Systems, cat. no. 746-LF-025)
- Activin-A (R&D Systems, cat. no. 338-AC-025)
- DAPT (Calbiochem, cat. no. 565770)
- Acidic FGF (aFGF) (R&D Systems, cat. no. 232-FA-025)
- Basic FGF (bFGF) (Upstate, cat. no. 01-106)
- Shh (R&D Systems, cat. no. 1314-SH-025)
- Taurine (Sigma, cat. no. T-8691)
- All-*trans* RA (Sigma, cat. no. R2625) ▲ **CRITICAL** Store in light-proof vials because RA is light sensitive.
- Laminin (BD Biosciences, cat. no. 35-4239)
- Fibronectin (GIBCO, cat. no. 33016-015)
- Y-27632 (Calbiochem, cat. no. 688001)

EQUIPMENT

- Water bath
- Centrifuge

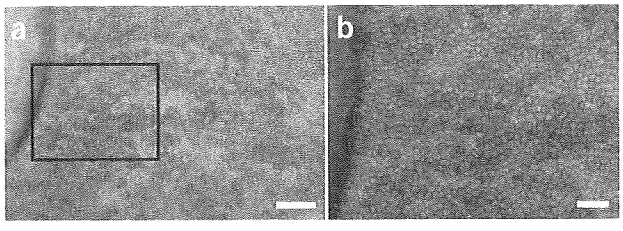

Figure 10 | Morphology of RPE cells differentiated from human ES cells. Pigmented cells begin to form ~40 d after initiation of differentiation. On day 120, pigmented cells form a single layer on the culture dish (**a**). Polygonal cells at various pigmentation stages are observed. Magnified image of pigmented cells in the boxed region of panel a (**b**). Scale bar, 100 μm (**a**) or 30 μm (**b**).

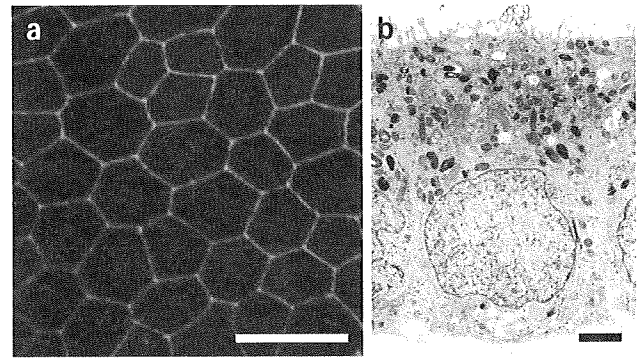

Figure 11 | RPE derived from human ES cells. Formation of tight junctions positive for ZO-1 on day 120 (**a**). Electron micrograph of human ES cell-derived pigmented cells on day 120 (**b**). Scale bar, 20 μm (**a**) or 100 nm (**b**). (Reproduced with permission from ref. 26).

- 100-mm dish (Falcon, cat. no. 35-3003)
- Petri dish (BIOBIK, cat. no. I-90)
- Low cell binding MPC-treated dish (NUNC, cat. no. 145401)
- Tubes (15 ml, 50 ml) (Falcon, cat. nos. 352095 and 352070)
- Disposable sterile filter system (0.22 μm) (Millipore, cat. no. SCGPU05RE)
- Plastic disposable transfer pipettes (5, 10, 25 and 50 ml) (Corning Costar, cat. nos. 4487, 4488, 4489 and 4490, respectively)
- Glass Pasteur pipette (IWAKI, cat. no. IK-PAS-9P)
- Eight-well chamber slide pre-coated with poly-D-lysine (BD BioCoat, cat. no. 354632)
- Tube with cell strainer (BD Biosciences, cat. no. 352235)
- Phase contrast microscope (Carl Zeiss)
- FACS machine (BD Biosciences)

REAGENT SETUP

Gelatin-coated dish

(1) Dissolve 500 mg of gelatin in 500 ml of dH_2O and autoclave at 121 °C for 20 min. The gelatin solution can be stored at room temperature (20–25 °C) for several months.
(2) For preparation of gelatin-coated dish, add 7 ml of gelatin solution to a 100-mm dish and let sit for at least 1 h.
(3) Dishes containing gelatin solution can be stored in a humidified incubator for several days. Storage for a longer period induces evaporation of gelatin solution even in a humidified incubator.
(4) Before use, aspirate the gelatin solution from the dish.

Poly-D-lysine/fibronectin/laminin-coated dish For the preparation of dishes coated with poly-D-lysine/fibronectin/laminin, we use poly-D-lysine-coated eight-well chamber slides.

(1) Mix 800 μl of 60 μg ml^{-1} laminin and 8 μl of 1 mg ml^{-1} fibronectin.
(2) Apply 100 μl of the mixture to each well of poly-D-lysine-coated eight-well chamber slide.
(3) Incubate the eight-well slide at 37 °C overnight.
(4) Add 500 μl of PBS to each well of the coated slide. Slides containing PBS can be stored in a humidified incubator for several days.
(5) Before use, aspirate the PBS from the wells.

The media for culturing mouse ES cells are shown in the tables below:

- Media for mouse ES cell maintenance

Component	Volume (ml)	Final concentration
GMEM	500	
Non-essential amino acid solution	5.8	0.1 mM
Pyruvate	5.8	1 mM
2-ME solution	0.58	0.1 mM
KSR	58	10%
FBS	5.8	1%

- Media for differentiation of mouse ES cells into retinal progenitors

Component	Volume (ml)	Final concentration
GMEM	500	
Non-essential amino acid solution	5.1	0.1 mM
Pyruvate	5.1	1 mM
2-ME solution	0.51	0.1 mM
KSR	28	5%

- Media for differentiation of mouse ES cells into retinal cells

Component	Volume (ml)	Final concentration
MEM-E HEPES	130	66%
HBSS	25	33%
Glucose solution	40	5.75 mg ml^{-1}
L-Glutamine	0.2	200 μM
N2 supplement	2	1%
FBS	2	1%
Penicillin/streptomycin	1	25 U ml^{-1}/25 mg ml^{-1}

Filter each medium using a 0.22-μm filter. Store the media at 4 °C for up to a week or in small aliquots (e.g., in a 50-ml tube) at −20 °C for several months. ▲ **CRITICAL** Maintenance of pluripotency, proliferation and differentiation efficiency depends on KSR and FBS. We recommend testing several lots beforehand and using the best lot. Old media result in low differentiation efficiency.

The media for culturing human ES cells are shown in the table below:

- Media for human ES cell maintenance

Component	Volume (ml)	Final concentration
DMEM/F12	500	
Non-essential amino acid solution	6.3	0.1 mM
L-Glutamine	6.3	2 mM
2-ME	0.005	0.1 mM
KSR	125	20%

- Media for human ES cell differentiation (20% KSR)

Component	Volume (ml)	Final concentration
GMEM	500	
Non-essential amino acid solution	6.6	0.1 mM
Pyruvate	6.6	1 mM
2-ME solution	0.66	0.1 mM
KSR	127	20%
Penicillin/streptomycin	5.0	50 U ml^{-1}/50 mg ml^{-1}

- Media for human ES cell differentiation (15% KSR)

Component	Volume (ml)	Final concentration
GMEM	500	
Non-essential amino acid solution	6.2	0.1 mM
Pyruvate	6.2	1 mM
2-ME solution	0.64	0.1 mM
KSR	93	15%
Penicillin/streptomycin	5.0	50 U ml^{-1}/50 mg ml^{-1}

- Media for human ES cell differentiation (10% KSR)

Component	Volume (ml)	Final concentration
GMEM	500	
Non-essential amino acid solution	5.5	0.1 mM
Pyruvate	5.5	1 mM
2-ME solution	0.58	0.1 mM
KSR	58.4	10%
Penicillin/streptomycin	5.0	50 U ml^{-1}/50 mg ml^{-1}

- Media for differentiation of human ES cells into photoreceptors

Component	Volume (ml)	Final concentration
GMEM	500	
Non-essential amino acid solution	5.5	0.1 mM
Pyruvate	5.5	1 mM
2-ME solution	0.56	0.1 mM
KSR	28	5%
N2 supplement	5.6	1%
Penicillin/streptomycin	5.0	50 U ml^{-1}/50 mg ml^{-1}

- Media for MEF

Component	Volume (ml)	Final concentration
DMEM	500	
FBS	55.5	10%

Filter each media using a 0.22-μm filter. Store at 4 °C for up to a week or in small aliquots (e.g., in a 50-ml tube) at −20 °C for several months. ▲ **CRITICAL** Maintenance of pluripotency, proliferation and differentiation efficiency depends on KSR. We recommend testing several lots beforehand and using the best lot. Old media result in low differentiation efficiency.

Human ES cell dissociation solution Dissolve collagenase IV in PBS at 10 mg ml^{-1} to produce the collagenase solution. Dissolve $CaCl_2/2H_2O$ in PBS at 100 mM to produce the $CaCl_2$ solution. Mix 10 ml of 2.5% (wt/vol) trypsin, 10 ml of collagenase solution, 1 ml of $CaCl_2$ solution, 20 ml of KSR and 59 ml of PBS, and filter using a 0.22-μm filter. Store small aliquots at −20 °C for several months.

2-ME solution Mix 14.1 ml of PBS and 0.1 ml of 2-ME. Prepare freshly before the preparation of media.

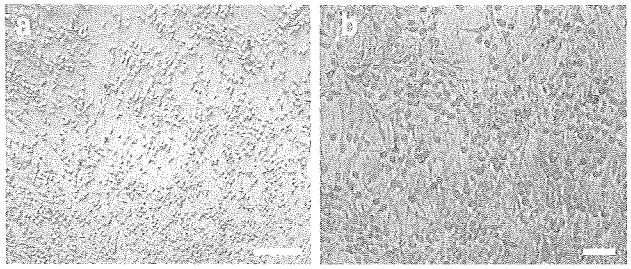

Figure 12 | Morphology of putative photoreceptors differentiated from human ES cells. Many neuron-like cells are observed on day 150 (**a**), although photoreceptors cannot be identified without staining. Magnified image of neuron-like cells (**b**). Scale bar, 100 μm (**a**) or 30 μm (**b**).

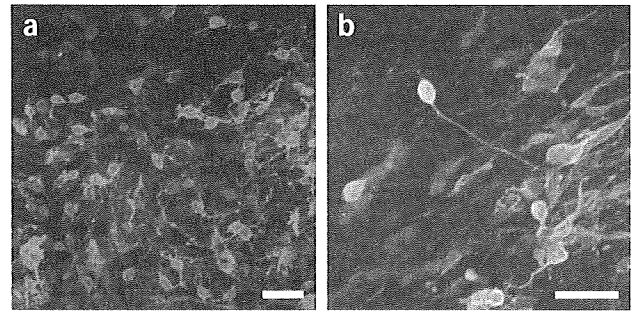

Figure 13 | Photoreceptors derived from human ES cells. Rhodopsin+ cells (red) are observed on day 150 (**a**). Rhodopsin+ cells (red) coexpress recoverin (green) on day 150 (**b**). Scale bar, 20 μm. (Reproduced with permission from ref. 26.)

Glucose solution Dissolve 1 g of glucose in 40 ml of HBSS in a 50-ml test tube. Prepare freshly before the preparation of media.
Blasticidin solution Dissolve blasticidin in dH_2O to a final concentration of 10 mg ml^{-1} and filter using a 0.22-μm filter. Store at 4 °C for up to several weeks or −80 °C for 6 months.
LIF solution Add 50 μl of LIF to 450 μl of PBS.
0.1% (wt/vol) BSA–PBS solution Dissolve 200 mg of BSA in 20 ml of PBS and filter using a 0.22-μm filter to produce a 1% (wt/vol) BSA–PBS. Mix 1 ml of 1% (wt/vol) BSA–PBS and 9 ml of PBS and filter using a 0.22-μm filter. Store at 4 °C for several weeks.
Dkk-1 solution Dissolve 10 μg (one vial) of Dkk-1 in 100 μl of 0.1% (wt/vol) BSA–PBS to produce a 100 μg ml^{-1} solution. Store at 4 °C for up to 1 week or −80 °C for several months.
Lefty-A solution Dissolve 25 μg (one vial) of Lefty-A in 100 μl of 0.1% (wt/vol) BSA–PBS to produce a 250 μg ml^{-1} solution. Store at 4 °C for up to 1 week or −80 °C for several months.
Activin-A solution Dissolve 25 μg (one vial) of Activin-A in 500 μl of 0.1% (wt/vol) BSA–PBS to produce a 50 μg ml^{-1} solution. Store at 4 °C for up to 1 week or −80 °C for several months.
aFGF solution Dissolve 25 μg (one vial) of aFGF in 500 μl of 0.1% (wt/vol) BSA–PBS to produce a 50 μg ml^{-1} solution. Store at 4 °C for up to 1 week or −80 °C for several months.
bFGF solution For mouse ES cells, mix 5 μl of 1 mg ml^{-1} bFGF and 500 μl of 0.1% (wt/vol) BSA–PBS to produce a 10 μg ml^{-1} solution. Store at 4 °C for up to 1 week or −80 °C for several months.
bFGF solution For human ES cells, mix 2.5 μl of 1 mg ml^{-1} bFGF and 500 μl of human ES cell maintenance media to produce a 5 μg ml^{-1} solution. Store at 4 °C for up to 1 week or −80 °C for several months.
Shh solution Dissolve 25 μg (one vial) of Shh in 500 μl of 0.1% (wt/vol) BSA–PBS to produce a 2.5 μM solution. Store at 4 °C for up to 1 week or −80 °C for several months.
Taurine solution Prepare a 50 mM solution in dH_2O and filter using a 0.22-μm filter. Store at 4 °C for up to 1 week or −80 °C for several months.
RA solution Prepare a 100 mM solution in DMSO. Store at 4 °C for up to 1 week or −80 °C for several months. Before use, dilute 100 mM RA solution with differentiation media to produce 100 μM solution.
DAPT solution Prepare a 10 mM solution in DMSO. Store at 4 °C for up to 1 week or −80 °C for several months.
Y-27632 solution Prepare a 10 mM solution in dH_2O and filter using a 0.22-μm filter. Store at 4 °C for up to 1 week or at −80 °C for several months.
Mitomycin C solution Prepare a 1 mg ml^{-1} solution in dH_2O and filter using a 0.22-μm filter. Store at −80 °C for several months.
PI solution Dissolve PI in ethanol at 10 mg ml^{-1}. Store at 4 °C up to 1 week or at −80 °C for several months.
MEF freezing solution Mix 8 ml of DMEM, 1 ml of FBS and 1 ml of DMSO. Prepare freshly before use.

EQUIPMENT SETUP

FACS In our laboratory, the FACSAria (Becton Dickinson) was used for analysis, counting and sorting of GFP-expressing cells. The entire process of cell sorting should be performed at room temperature. Excitation of GFP should be performed at a wavelength of 488 nm and fluorescence emission should be detected using a band pass filter of 530 nm (FITC). Cells should be sorted at low speed (<4,000 cells per s) using a wide nozzle (100 μm). Cell aggregates and PI-positive dead cells should be gated out using forward scatter and side scatter parameters and a band pass filter of 695 nm (PerCP-Cy5.5). Data analysis was performed using FACSDiva software (BD Biosciences).

PROCEDURE

1| Obtain mouse or human ES cells as described earlier[26,45,47].

2| Differentiation of ES cells to retinal cells can be performed using option A for mouse ES cells or option B for human ES cells.

(A) Retinal differentiation from mouse Rx-GFP ES cells (day 0: maintenance and passaging of cells ● TIMING 1.5 h)

(i) To maintain and passage ES cells, aspirate the media from a confluent 100 mm dish of mouse ES cells, then add 9 ml of pre-warmed PBS (37 °C). Remove the PBS, and add 1 ml of pre-warmed (37 °C) 0.25% (wt/vol) trypsin-EDTA and incubate the dish at 37 °C for 5 min.

(ii) Add 2 ml of retinal progenitor differentiation media to the dish, and dissociate the ES colonies into single cells by pipetting with a P1000 Pipetman. Transfer the cell suspension to a 15-ml conical tube.

(iii) To collect the remaining cells in the dish, add 2 ml of retinal progenitor differentiation media to the dish, and transfer the cell suspension into the 15-ml conical tube.

(iv) Centrifuge the 15-ml tube for 3 min at 180*g* at room temperature.

(v) Aspirate the supernatant and add 2 ml of retinal progenitor differentiation media to resuspend the cells.
▲ **CRITICAL STEP** Do not use the maintenance media to resuspend cells for differentiation experiments because the maintenance media contain FBS, which inhibits neural differentiation.

(vi) Mix 50 μl of the cell suspension and 50 μl of 0.4% (wt/vol) Trypan blue and count the number of cells using a cell counter.